IEEE Access
Multidisciplinary | Rapid Review | Open Access Journal

Received February 16, 2021, accepted February 24, 2021, date of publication February 26, 2021, date of current version March 9, 2021.

Digital Object Identifier 10.1109/ACCESS.2021.3062769

An Approach for Optimal Pre-Conditioning of the Analytical Field Solution of Slotless PM Machines

MATTEO LEANDRO, (Member, IEEE), AND JONAS KRISTIANSEN NØLAND, (Member, IEEE)
Department of Electric Power Engineering, Norwegian University of Science and Technology, 7491 Trondheim, Norway
Corresponding author: Matteo Leandro (matteo.leandro@ntnu.no)

ABSTRACT Analytical modeling of electrical machines has the advantage of remarkable computational efficiency when compared with finite element analysis (FEA). This is especially important for slotless topologies, as they are well suited for 2-D analytical field solutions. Nevertheless, the analytical techniques are doubtlessly non-trivial; besides, the ill-conditioned nature of the problem comes along with the mathematical complexity. The numerical issues are shown to be loosely assessed or even ignored in some parts of the literature, which causes a lack of replicability and low practical usability of analytical approaches. Although researchers often adopt a numerically optimized formulation in their works, the mathematical manipulations that make the solutions to be well-posed and efficiently exploitable are often hidden from the reader since the focus is rather on the theoretical derivation and the exact solutions. This paper shows how the direct field solution of the magnetic field problem, named the raw field formulation (RFF), can lead to significant errors throughout the domain of slotless SPM machines, which vary significantly with the machine geometry. Then, an approach to reach the numerically optimal form of the field solution, named optimized field formulation (OFF), is proposed, comprehensibly described, and discussed. Finally, the closed-form expression and the optimal pre-conditioner underneath are explicitly presented and shown to outperform the accuracy of other pre-conditioned formulations used in the literature (including RFF). The OFF's performance is significant, especially at higher harmonic orders.

INDEX TERMS Analytical solutions, numerical precision, permanent magnet machines, slotless machines.

NOMENCLATURE

The nomenclature of this paper is adopted from well-known terminology, where the variables are described in the following.

α_m	Mid-magnet span angle [rad]
α_p	Mid-magnet to pole angle ratio
$\boldsymbol{B}$	Magnetic flux density vector [T]
$\boldsymbol{H}$	Magnetic field strength [A/m]
$\boldsymbol{M}$	Magnetization vector [A/m]
μ_0	Free-space permeability [A/m]
μ_r	PM recoil (relative) permeability
ω	electrical angular frequency [rad/s]
b	parallel ways per phase
B_{rem}	PM remanent flux density [T]
I	phase current peak value [A]
m	space harmonics order from armature field
n	space harmonics order from PMs field
N_t	number of conductors per coil
n_{max}	PMs field harmonic order at truncation
p	Number of pole pairs
q	coils per pole and per phase
l_a	Machine active length [mm]
R_s	Iron boundary contiguous to winding [mm]
R_g	Mid-airgap radius [mm]
R_i	Iron boundary contiguous to magnets [mm]
R_m	Magnets boundary facing the winding [mm]
R_r	Magnets boundary contiguous to iron boundary [mm]
R_{wi}	Winding boundary contiguous to iron boundary [mm]
R_w	Winding boundary facing the magnets [mm]

Superscripts

J	armature reaction contribution
PM	PM contribution

The associate editor coordinating the review of this manuscript and approving it for publication was Wen-Sheng Zhao.

Subscripts

- ϑ Circumferential component (mechanical angle) [rad]
- r Radial component
- z Axial or z component

I. INTRODUCTION

Slotless permanent magnet (PM) machines have been shown to provide interesting features and performances in several application areas. It allows for lightweight designs [1], high-specific-power machines [2], high-speed performance [3], and reduced iron losses [4]. The machine typology can be studied analytically, which makes very efficient design optimizations feasible.

The advanced design of rotating electrical machines will often involve multi-objective optimizations, with goals that may differ between machine topologies. Regardless of topology, the design tool usually has to generate a reliable and accurate solution, along with appropriate computational performance. Any lack of precision will impose errors when characterizing the machine with respect to the machine rating, i.e., inductance, torque, as well as internal forces, and stresses. The latter necessity has brought attention towards analytical modeling, as it ensures comparable accuracy to the finite element analysis (FEA), in those cases where magnetic saturation does not have a significant impact, such as in ultra-high-speed machines where magnetic loading is maintained very low to limit magnetic losses. Most of the FE-based commercial software or custom-made reluctance network implementations [5] ensure built-in flexibility. The FE also provides a strongly coupled multiphysics functionality, but in a black box numerical environment where parametric relationships are not directly seen. Nevertheless, analytical models' use becomes certainly preferable as it contains all the required information expressed in direct mathematical relationships, which may lead to important advantages for sensitivity analyses and optimization procedures. In some instances, the same analytical model can be extended to account for low iron permeability [6] or even to include iron core saturation through iterative methods [7]–[9]. Additionally, the problem's mathematical structure allows the analysis to be extended to rotor eccentricity through conformal mapping [10]–[12] while preserving the high numerical performance inherent in analytical models. However, there will always be a risk of poorly formulated analytical expressions that creates significant numerical errors [13]–[15].

With a particular focus on the analytical field solution's numerical performance, the paper aims to highlight an issue that tends to be overlooked in the current literature. This may lead to a lack of reproducibility of analytical frameworks proposed by the authors, although they are theoretically exact. The definition of the classical problem through the so-called subdomain model allows extending the same methodology, used for slotless machine geometries, to the slotted topology [16]–[22]. Despite the paper's focus on slotless topologies, the way to tackle the problem is similar when modeling slotted topologies as well.

A. CONTRIBUTION OF THE PAPER

In this article, different case studies for the slotless machine topology are used to address the described numerical issue. The broadly adopted two-dimensional (2-D) Fourier-based method for solving Maxwell's equations [14], [23], [24], is developed with regard to its numerical performance. In order to define a generally exploitable slotless topology, the basis for the field problem definition is the one depicted in Fig. 1. It is an extension of what is reported in [25], where only the PM field solution was studied. The different case studies, that can be modeled according to the definition of Fig. 1, are summarized in Table 1. The distinction between the in-runner and the out-runner topology is needed for the implementation of the OFF for the two cases. The paper's rationale is built upon the current literature contributions, with a particular focus on the structure of the presented formulations. By first classifying the different formulations being presented, the link between them is outlined by defining the formulations from scratch. The aim is to prevent other researchers from stumbling upon this numerical issue when trying to develop, replicate, and reproduce similar problems exhibiting the same issue. The final goal is defining a rationally-constructed methodology to tackle the problem and to outline the criterion to extend it to similar problems, i.e., slotted topologies. It is worth to stressing that the scope of the paper is to address the numerical issue deriving from the development of these analytical models rather than presenting the analytical models per se.

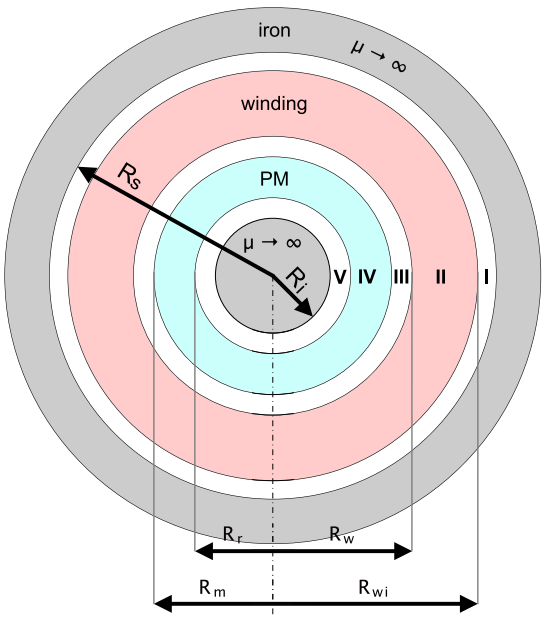

FIGURE 1. Reference subdomain/layers subdivision of a slotless PM machine, for field formulation.

TABLE 1. Parameter definition of the different case study.

		INRUNNER	OUTRUNNER
		$R_s > R_w > R_m > R_r > R_i$	$R_i > R_r > R_m > R_w > R_s$
Iron-cored	single airgap	$R_s = R_{we}$	$R_i = R_r$
	double airgap	$R_s > R_{we}$; $R_i = R_r$	$R_s < R_{we}$; $R_i = R_r$
Air-cored	single airgap	$R_s = R_{we}$ $R_i = 0$	$R_s = R_{we}$ $R_i = \infty$
	double airgap	$R_s > R_{we}$; $R_i = 0$	$R_s < R_{we}$; $R_i = \infty$
	fully air-cored	$R_s = \infty$; $R_i = 0$	$R_s = 0$; $R_i = \infty$

B. OUTLINE

The remaining part of the paper is structured as follows. A literature review is conducted in Section II to guide the reader through the proposed classification. Then, in Section III, the magnetic field problem is briefly defined. The magnetic field contribution from PMs is expressed in Section IV. The problem is then solved, and the RFF is presented. Moreover, the link between the RFF and the OFF is highlighted. The assessment of the different achieved accuracy levels is analyzed in Section V, with particular regard to machine parameters' dependency. In Section VI, the magnetic field contribution from the armature current is added. Finally, the numerical sensitivity analysis and the problem impact on the results are presented in Sections VII and VIII, respectively. Different examples are considered as a case study to address the numerical issue. Section VIII concludes the paper.

II. REVIEW OF THE NUMERICAL ISSUE

We will first give an introduction to the occurrence of the numerical issue. The procedure for obtaining the resolution of the field problem (as will be detailed in the following section) leads to an inherent lack of accuracy in the final formulation when numerically implemented. In any case, the final field formulations are expressed as a Fourier series accounting for all the space harmonics introduced by the sources in the given domain. The harmonic amplitudes are what have to be found by means of the boundary conditions. As noted in reference [13], the resulting system of equations appears to become ill-conditioned with the increase of the harmonic order. It is physically reasonable to observe the decay of the amplitude for high order harmonics. This is because the magnets/winding distribution is configured in such a way that the fundamental components dominate high order harmonics. However, it can be shown that the mere implementation of the RFF exhibits a lack of accuracy when compared to FEA. This suggests that the problem is an intrinsic consequence of the ill-condition nature of the mathematical model; thus, it goes beyond the physical meaning mentioned beforehand.

This limitation was mentioned in [14], [15], both referring to the work presented in [13]. A potentially misleading comparison between analytical-based and FE-based field solutions for a radial flux rotating machine (Fig. 14 and 15 in [13]) suggests the latter to be more accurate than the former one. The effect of the ill-conditioned nature of the system is clearly visible in the magnet's region. In the same work, a solution for mitigating the problem is proposed. The suggestion is to use some scaling factors to reduce the condition number of the resulting system of equations. However, as it will be noted, relying on these scaling factors without first knowing where the inaccuracy is generating from may lead to sub-optimal formulations like those adopted in [26]. It is worth mentioning that, in [13], different analytical formulations based on different coordinate systems are investigated without emphasizing the possibility to overcome the mentioned issue. In reference [27], a proper scaling methodology is adopted to solve the problem in Cartesian coordinates.

As shown, there is a need to assess and deal with this issue in more detail, since the RFF and the OFF are presented interchangeably in the current literature. It is worth mentioning that both of the formulations are an exact solution to the field problem, and thus, they are mathematically equivalent. The subtle difference between the two expressions lies only in the algebraic representation, which results in different numerical performances. The main reason why some authors have decided to present the RFF instead of an OFF, may be due to the former expressions' compactness. In fact, the RFF does not generally require to distinguish the in-runner from the out-runner case.

Authors in [28]–[30] have presented a thorough field problem definition, showing the RFF as the final formulation. Nevertheless, the perfect correspondence between the analytical solution and FEA clearly suggests that the OFF was adopted in the simulations. In fact, as it will be noted, the inaccuracy in the RFF increases with the increase in the number of poles, and in the aforementioned contributions, the pole-counts of the case studies was rather high. Similarly, in reference [31], the explicit expressions shown in the appendix suggest them to be RFFs. However, given that a 30-pole machine was taken as a case study (whereby the final inaccuracy would be remarkable), it is likely that the OFF was adopted. A comparison with FE is missing to prove the latter statement.

Admittedly, there are several publications in which the OFF is adopted and shown for the final formulations. However, these mathematical expressions are not the natural outcome of the solution to Maxwell's equations. Thus, it becomes difficult to replicate their analytical modeling based on the provided information. Only a few contributions specify that the presented expressions are the result of some algebraic manipulations. Nevertheless, the idea behind the rearrangement of these expressions is hidden.

It is of paramount concern to address the inaccuracy highlighted in [13] as a fictitious and avoidable issue. Considering, for example, the PM demagnetization analysis by means of analytical modeling presented in [32], the numerical inaccuracy might lead to the impossibility of carrying out the analysis through analytical modeling.

One could argue that dealing with ill-conditioned system is a rather common practice in several scientific fields. Nevertheless, the optimal solution to overcome this problem and conveniently condition the original mathematical system lies in the understanding of the problem's origins.

In Table 2, some contributions from the literature are gathered and classified. They are arranged according to those using the RFF from those expressing the OFF, and those which do not show any expression. With regard to the latter category, it is worth mentioning that in [6], the expressions of the explicit formulations are not shown. However, given that a perfectly sinusoidal field distribution from the magnets was assumed, the use of the RFF or the OFF would make no difference. In fact, in such a case, any inaccuracy from the RFF is hidden by the absence of any harmonic component. The latter remark holds for the work presented in [33] as well, where the same case study was considered.

TABLE 2. Numerical issue assessment in the literature.

RFF	OFF	Not Stated
[28]–[31]	[34]–[38]	[4], [6], [32], [33]

III. PROBLEM FORMULATION

The two-dimensional analytical field solution for rotating electrical machines holds under specific assumptions that help to simplify the differential equations governing the field problem itself. As it will be noted, these assumptions may get representative of some real practical examples when specific design requirements are met (e.g., low saturation level). The starting assumptions are listed below, along with their effect on the problem definition.

1) The problem is described in polar coordinates (r, ϑ, z).
2) The field map lies on the (r, ϑ) plane, with no variation assumed along the rotational axis (z-direction) leading to a 2-D field map. The flux conservation law ($\nabla \cdot \boldsymbol{B} = 0$) allows to define the magnetic vector potential ($\boldsymbol{A}$) as: $\boldsymbol{B} = \nabla \times \boldsymbol{A}$; which entails the vector potential to have the only z-component. Another direct consequence is that end-effects are neglected; thus, the current density vector ($\boldsymbol{J}$) is described by its only z-component
3) The iron has infinite permeability, and the magnetic saturation is neglected (linear material property).The on-load field solution can be found through superposition principle, by summing PMs field and armature reaction field.
4) The PMs are uniformly magnetized.
5) The stator coils are arranged as a three-phase winding (following the model described in [28]) over a single layer, with each phase belt covering 60 electrical degrees. In the winding region, a uniform current density distribution is assumed.
6) The three-phase current is assumed to be sinusoidal and expressed as it follows.

$$i_a(t) = I\cos\omega t \tag{1}$$
$$i_b(t) = I\cos\omega t - 2\pi/3 \tag{2}$$
$$i_c(t) = I\cos\omega t + 2\pi/3 \tag{3}$$

The problem can be fully described by the Ampère's law, which is defined for each region as it follows.

$$\begin{aligned} \nabla \times \boldsymbol{H} = \boldsymbol{J} &\rightarrow \begin{cases} \boldsymbol{J} = 0 & \text{Air \& PM} \\ \boldsymbol{J} \neq 0 & \text{Winding} \end{cases} \\ \boldsymbol{H} = \frac{\boldsymbol{B}}{\mu_0\mu_r} - \frac{\boldsymbol{M}}{\mu_r} &\rightarrow \begin{cases} \boldsymbol{M} = 0 & \text{Air \& Winding} \\ \boldsymbol{M} \neq 0 & \text{PM} \end{cases} \end{aligned} \tag{4}$$

By using the above equation, along with the definition of the magnetic vector potential, under the given assumptions, one can end up reframing the problem as in eq. (5).

$$\nabla^2 A_z = \begin{cases} 0 & \text{Air-regions} \\ -\mu_0 J_z & \text{Winding-region} \\ -\mu_0 \nabla \times \boldsymbol{M} & \text{PM-region} \end{cases} \tag{5}$$

The obtained Laplace's equation (for the air region) and Poisson's equations (where PMs magnetization or winding currents are acting), can be solved by means of the method of separation of variables. The contributions from the PMs field and current field are considered separately by applying the superposition principle. This means that when considering the contribution from the PM field, in the winding region, the governing equation is the Laplace's one (i.e., $J_z = 0$); vice versa, for the current field contribution, in the PM region the Laplace's equation holds (i.e., $\boldsymbol{M} = 0$). For this latter case, another assumption is made, which simplifies the model definition as follows.

- The PM's relative permeability (μ_r) is assumed to be unitary for the definition of the stator current field contribution.

IV. MAGNETIC FIELD CONTRIBUTION FROM PMs

This section presents the field contribution of the PMs. The vast majority of the authors have adopted the direct definition of the magnetization distribution, as it is most intuitive. As an alternative, some authors have modeled the magnetization with a suitable equivalent surface current density acting on each magnet boundary ([28], [29]). In the most common case, once the topology of the magnets array is set, the resulting magnetization is defined mathematically as a Fourier series for both radial and circumferential components ([19], [36], [39]–[42]), as it follows:

$$M_r = \sum_{n=p,3p,5p,\ldots}^{\infty} M_{rn}\cos(n\vartheta) \tag{6}$$

$$M_\vartheta = \sum_{n=p,3p,5p,\ldots}^{\infty} M_{\vartheta n}\sin(n\vartheta) \tag{7}$$

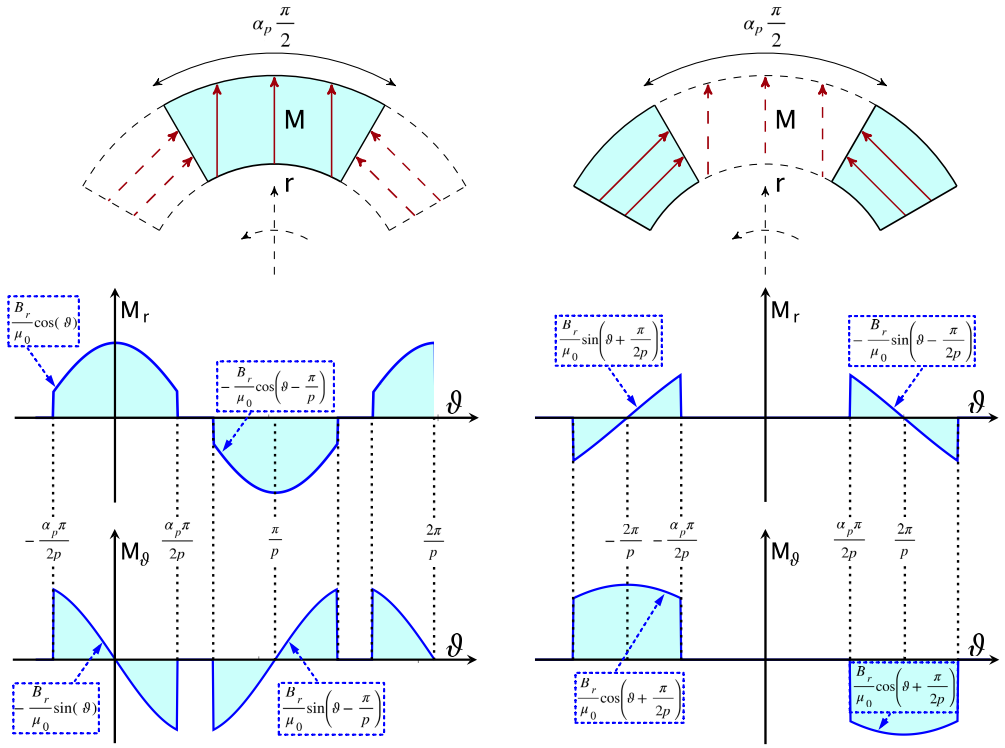

(a) Mid-magnets **(b)** Side-magnets

FIGURE 2. **Illustration of 2-segments Halbach array with mid-magnet (a) and side-magnets (b) magnetization distribution (typical waveforms of a 2-poles inrunner machine).**

The right hand side term of eq. (5), i.e., the Poisson's equation, can be rewritten, yielding to:

$$\mu_0 \nabla \times \boldsymbol{M} = \frac{1}{r}\left(\frac{\partial (rM_\vartheta)}{\partial r} - \frac{\partial M_r}{\partial \vartheta}\right) = \frac{1}{r}\left(M_\vartheta - \frac{\partial M_r}{\partial \vartheta}\right) = \frac{\mu_0}{r} \sum_{n=p,3p,5p,\ldots}^{\infty} [M_{\vartheta n} + nM_{rn}] \sin(n\vartheta). \quad (8)$$

The left hand side term is explicitly written and conveniently rearranged in order to apply the method of separation of variables. The resulting Poisson's equation is then expressed as:

$$r\frac{\partial A_{z,\mathrm{IV}}^{\mathrm{PM}}}{\partial r} + r^2 \frac{\partial^2 A_{z,\mathrm{IV}}^{\mathrm{PM}}}{\partial r^2} + \frac{\partial^2 A_{z,\mathrm{IV}}^{\mathrm{PM}}}{\partial \vartheta^2} = -r\mu_0 \sum_{n=p,3p,5p,\ldots}^{\infty} [M_{\vartheta n} + nM_{rn}] \sin(n\vartheta), \quad (9)$$

which is the governing differential equation in the magnets region for any type of magnets arrangement.

Given the several attractive features that Halbach arrays exhibit [43], the considered case study involves a two-segmented Halbach array (as classified in [39]). The parallel magnetization in each magnet segment is considered for the implementation, as the cylindrical magnetization is rather uncommon to be manufactured. A single section of a two segments Halbach array is depicted in Fig. 2 to help defining the resulting magnetization distribution as described in Appendix A. The same procedure can be adopted for other magnets arrangement, and the only thing changing is the coefficients in M_{rn} and $M_{\vartheta m}$.

The field solution for regions I, II, and III can be studied as a single domain solution, as no variation in the magnetic properties is expected between the three regions. Therefore, in the following, a single airgap region (named III) is considered for the sake of simplicity. According to eq. (5) in region III and V, the governing differential equation is the following.

$$r\frac{\partial A_z^{\mathrm{PM}}}{\partial r} + r^2 \frac{\partial^2 A_z^{\mathrm{PM}}}{\partial r^2} + \frac{\partial^2 A_z^{\mathrm{PM}}}{\partial \vartheta^2} = 0 \quad (10)$$

The Laplace equation, as written in eq. (10), can be solved by means of the method of separation of variables, which yields

$$A_z^{\mathrm{PM}}(r,\vartheta) = \sum_{n=p,3p,5p,\ldots}^{\infty} [A_{z,n}^{+} r^n + A_{z,n}^{-} r^{-n}] \sin(n\vartheta), \quad (11)$$

while the solution to eq. (9) requires to add a particular solution to the homogeneous solution in eq. (11), yielding

$$A_{z,\mathrm{IV}}^{\mathrm{PM}}(r,\vartheta) = \sum_{n}^{\infty} [A_{z,\mathrm{IV}}^{m+} r^n + A_{z,\mathrm{IV}}^{m-} r^{-n} + A_{\mathrm{PM}}(r)] \sin(n\vartheta). \quad (12)$$

In eq. (12), $A_{\mathrm{PM}}(r)$ is defined for any n according to

$$A_{\mathrm{PM}}(r) = \begin{cases} \dfrac{\mu_0(M_{\vartheta n} + nM_{rn})}{(n^2-1)} \cdot r & \text{if } n \neq 1 \\ -\dfrac{\mu_0}{2}(M_{r1} + M_{\vartheta 1}) \cdot r \ln(r) & \text{if } n = 1. \end{cases} \tag{13}$$

The distinction of cases is necessary as the case $n = 1$, namely the fundamental component of a 2-pole machine, would otherwise exhibit a singularity.

The field solutions in the three regions are related and bounded by the following boundary conditions.

$$H^{\mathrm{PM}}_{\vartheta,\mathrm{III}}\Big|_{r=R_s} = 0 \tag{14}$$

$$\left(B^{\mathrm{PM}}_{r,\mathrm{III}} = B^{\mathrm{PM}}_{r,\mathrm{IV}}\right)\Big|_{r=R_m}, \quad \left(H^{\mathrm{PM}}_{\vartheta,\mathrm{III}} = H^{\mathrm{PM}}_{\vartheta,\mathrm{IV}}\right)\Big|_{r=R_m} \tag{15}$$

$$\left(B^{\mathrm{PM}}_{r,\mathrm{IV}} = B^{\mathrm{PM}}_{r,\mathrm{V}}\right)\Big|_{r=R_r}, \quad \left(H^{\mathrm{PM}}_{\vartheta,\mathrm{IV}} = H^{\mathrm{PM}}_{\vartheta,\mathrm{V}}\right)\Big|_{r=R_r} \tag{16}$$

$$H^{\mathrm{PM}}_{\vartheta,\mathrm{V}}\Big|_{r=R_i} = 0 \tag{17}$$

Eqs. (14) and (17) are ensured by the assumed infinite iron permeability, while eqs. (15) and (16) set the continuity of the field solution in the whole domain, and they are ensured by the *interface conditions for electromagnetic fields*. The different expressions to be used in the above-written boundary conditions are reported in Appendix B. Consequently, a system of six equations in the six unknowns: $A^+_{z,\mathrm{III}}$, $A^-_{z,\mathrm{III}}$, $A^+_{z,\mathrm{IV}}$, $A^-_{z,\mathrm{IV}}$, $A^+_{z,\mathrm{V}}$, and $A^-_{z,\mathrm{V}}$, is defined for each and every one of the harmonic components ($n = p, 3p, 5p, \ldots$), yielding:

$$\begin{cases} A^+_{z,\mathrm{III}}R_s^{n-1} - A^-_{z,\mathrm{III}}R_s^{-n-1} = 0 \\ A^+_{z,\mathrm{III}}R_m^{n-1} + A^-_{z,\mathrm{III}}R_m^{-n-1} = \ldots \\ \qquad \ldots = A^+_{z,\mathrm{IV}}R_m^{n-1} + A^-_{z,\mathrm{IV}}R_m^{-n-1} + A_{\mathrm{PM},r}(R_m) \\ \mu_r n(A^+_{z,\mathrm{III}}R_m^{n-1} - A^-_{z,\mathrm{III}}R_m^{-n-1}) = \ldots \\ \quad \ldots = nA^+_{z,\mathrm{IV}}R_m^{n-1} - nA^-_{z,\mathrm{IV}}R_m^{-n-1} + A_{\mathrm{PM},\vartheta}(R_m) + \mu_0 M_{\vartheta n} \\ A^+_{z,\mathrm{V}}R_r^{n-1} + A^-_{z,\mathrm{V}}R_r^{-n-1} = \ldots \\ \qquad \ldots = A^+_{z,\mathrm{IV}}R_r^{n-1} + A^-_{z,\mathrm{IV}}R_r^{-n-1} + A_{\mathrm{PM},r}(R_r) \\ \mu_r n(A^+_{z,\mathrm{V}}R_r^{n-1} - A^-_{z,\mathrm{V}}R_r^{-n-1}) = \ldots \\ \quad \ldots = nA^+_{z,\mathrm{IV}}R_r^{n-1} - nA^-_{z,\mathrm{IV}}R_r^{-n-1} + A_{\mathrm{PM},\vartheta}(R_r) + \mu_0 M_{\vartheta n} \\ A^+_{z,\mathrm{V}}R_i^{n-1} - A^-_{z,\mathrm{V}}R_i^{-n-1} = 0. \end{cases} \tag{18}$$

The system is typically written in matrix form (as in (21)) and solved for a certain number of harmonics. In this case, to develop the closed form field expressions (as in [25], [29]), the symbolic notation is kept, and the system was solved in the Wolfram Cloud as it performs improved simplifications of the expressions with built-in commands. This approach can be advantageous when the solution is adopted in a design procedure where the field solution is needed only in specific regions. Thus, there would be no need to solve the whole domain's problem for different geometrical parameters. Moreover, the development of closed-form expressions will help to better frame the origins of the numerical problem and give a rigorous meaning to the proposed solution in this paper. Nevertheless, the matrix form will also be shown to meet the rationale of other researchers.

In the following, the only radial flux density solution in the winding/airgap region (III) will be considered for the closed-form expressions. This choice is driven by the fact that the airgap field allows assessing machine performances like torque and back-emf exhaustively ([41], [44]) and in a compact way. Moreover, the numerical inaccuracy can be observed in any derived field quantity interchangeably since they all relate to the solution of the linear system in (18). Thus, the radial component was chosen as a test function. The resulting coefficients in the winding/airgap region ($A^+_{z,\mathrm{III}}$, $A^-_{z,\mathrm{III}}$) when $n \neq 1$ are reported in (19). By plugging the two coefficients into (59)-(62) of Appendix B, one would get the so defined RFF which describes the magnets field solution of the general geometry shown in Fig. 1 and therefore, all the cases summarized in Table 1. The particular case with $n = 1$ requires a different system of equations to be solved, as the field expressions for the particular case have to be considered. However, the resulting system of equations does not suffer the same numerical issue, as the coefficient n is set to the lowest value ($n = 1$). For this reason, and for the sake of compactness, the solution for the particular case will not be included.

A. LINK BETWEEN RFF AND OFF

As mentioned in the introduction, the lack of accuracy in the RFF occurs as a numerical phenomenon once the expression is coded. The problem occurs within the expressions shown in eq. (19), as shown at the bottom of the next page. The numerical resolution requires the math coprocessor (in a computer) to perform multiplications and divisions between radii, which are raised to an exponent (n), which increases with the harmonic order and the number of pole pairs. In such a scenario, modeling machines with radii below or above one meter may cause underflow or overflow of the result, respectively, already at low harmonic order. In a similar instance, if the system is solved directly in its matrix form, the number of harmonics needs to be limited to a value such that the system is still well-conditioned.

The sensitivity to the size of the machine will be further addressed in the following. The idea behind the resolution of such a problem is to rearrange the entire field formulations in order to make the numerical performance of the OFF to be independent of the machine size; thus, meeting the uttermost level of generality. The different algebraic steps to obtain the OFF are summarized in Table 3, referring to the harmonics' amplitudes of the radial flux density component of eq. (59) in Appendix B.

From eq. (20), as shown at the bottom of the next page, it is clear how the amplitude of each harmonic is now dependent on ratios between radii rather than just radii (as in (19)); this helps both preventing elemental operations from exhibiting a quick underflow/overflow for high harmonic orders, and the model being size-independent. One can also notice that all the ratios between radii in eq. (20) are lower than one. It implies that once a ratio (as an elemental operation) causes underflow (i.e., is rounded to zero), there will always be a

TABLE 3. Link between *RFF* and *OFF* (radial flux density component).

	INRUNNER	OUTRUNNER
RFF →	$\underbrace{(59),(19)}$ ↓ $nA^{+}_{z,\mathrm{III}}[r^{n-1}+R_s^{2n}r^{-n-1}]$	
	$\underbrace{nA^{+}_{z,\mathrm{III}}\frac{R_s^{2n}}{R_m^{n+1}}\left[\left(\frac{r}{R_s}\right)^{n-1}\left(\frac{R_m}{R_s}\right)^{n+1}+\left(\frac{R_m}{r}\right)^{n+1}\right]}$ ↓ $\left(\frac{R_rR_m}{R_rR_m}\right)^{2n}nA^{+}_{z,\mathrm{III}}\frac{R_s^{2n}}{R_m^{n+1}}\left[\left(\frac{r}{R_s}\right)^{n-1}\left(\frac{R_m}{R_s}\right)^{n+1}+\left(\frac{R_m}{r}\right)^{n+1}\right]$	$\underbrace{nA^{+}_{z,\mathrm{III}}R_m^{n-1}\left[\left(\frac{r}{R_m}\right)^{n-1}+\left(\frac{R_s}{r}\right)^{n+1}\left(\frac{R_s}{R_m}\right)^{n-1}\right]}$ ↓ $\left(\frac{R_iR_rR_m}{R_iR_rR_m}\right)^{2n}nA^{+}_{z,\mathrm{III}}R_m^{n-1}\left[\left(\frac{r}{R_m}\right)^{n-1}+\left(\frac{R_s}{r}\right)^{n+1}\left(\frac{R_s}{R_m}\right)^{n-1}\right]$
OFF →	$K_B(n)f_{r,\mathrm{PM}}(r,n) \rightsquigarrow (20)$	$K_{B,out}(n)f_{r,out,\mathrm{PM}}(r,n)_r(r,n) \rightsquigarrow (20)$

finite term preventing the expression from collapsing to zero. For this reason, the out-runner case and the in-runner case must be treated separately. For the out-runner case, the in-runner expression would make all the ratios to become greater than one. Thus, high order harmonics would exhibit a quick overflow, which cannot be overwritten by other finite terms within the expression.

$$
\begin{aligned}
A^{+}_{z,\mathrm{III}} &= \frac{\begin{array}{l}R_m^n\{R_m^{2n+1}[R_r^{2n}(\mu_r+1)-R_i^{2n}(\mu_r-1)](nA^m_{z,n}-\mu_0M_{\vartheta n}-A^m_{z,n})\\ +R_mR_r^{2n}[R_r^{2n}(\mu_r-1)-R_i^{2n}(\mu_r+1)](nA^m_{z,n}+\mu_0M_{\vartheta n}+A^m_{z,n})\\ +2R_m^nR_r^{1+n}[R_r^{2n}(A^m_{z,n}-\mu_rnA^m_{z,n}+\mu_0M_{\vartheta n})+R_i^{2n}(A^m_{z,n}+\mu_rnA^m_{z,n}+\mu_0M_{\vartheta n})]\}\end{array}}{\begin{array}{l}n\{-R_m^{4n}(\mu_r-1)[R_r^{2n}(\mu_r+1)-R_i^{2n}(\mu_r-1)]+R_m^{2n}R_r^{2n}(\mu_r+1)[R_r^{2n}(\mu_r-1)-R_i^{2n}(\mu_r+1)]\\ +R_s^{2n}R_m^{2n}(\mu_r+1)[R_r^{2n}(\mu_r+1)-R_i^{2n}(\mu_r-1)]-R_r^{2n}R_s^{2n}(\mu_r-1)[R_r^{2n}(\mu_r-1)-R_i^{2n}(\mu_r+1)]\}\end{array}}\\
A^{+}_{z,\mathrm{III}} &= R_s^{2n}A^{+}_{z,\mathrm{III}}\\
K_B(n) &= \frac{\begin{array}{l}(nA^m_{z,n}-A^m_{z,n}-\mu_0M_{\vartheta n})\left[(\mu_r+1)-\left(\frac{R_i}{R_r}\right)^{2n}(\mu_r-1)\right]\\ +(nA^m_{z,n}+A^m_{z,n}+\mu_0M_{\vartheta n})\left[\left(\frac{R_r}{R_m}\right)^{2n}(\mu_r-1)-\left(\frac{R_i}{R_m}\right)^{2n}(\mu_r+1)\right]\\ +2\left(\frac{R_r}{R_m}\right)^{n+1}\left[(A^m_{z,n}+\mu_0M_{\vartheta n}-\mu_rnA^m_{z,n})+\left(\frac{R_i}{R_r}\right)^{n}(A^m_{z,n}+\mu_0M_{\vartheta n}+\mu_rnA^m_{z,n})\right]\end{array}}{\begin{array}{l}(\mu_r^2-1)\left[\left(\frac{R_i}{R_m}\right)^{2n}-\left(\frac{R_m}{R_s}\right)^{2n}+\left(\frac{R_r}{R_s}\right)^{2n}-\left(\frac{R_i}{R_r}\right)^{2n}\right]\\ +(\mu_r+1)^2\left[1-\left(\frac{R_i}{R_s}\right)^{2n}\right]+(\mu_r-1)^2\left[\left(\frac{R_m}{R_s}\right)^{2n}\left(\frac{R_i}{R_r}\right)^{2n}-\left(\frac{R_r}{R_m}\right)^{2n}\right]\end{array}}\\
K_{B,out}(n) &= \frac{\begin{array}{l}(nA^m_{z,n}-A^m_{z,n}-\mu_0M_{\vartheta n})\left[\left(\frac{R_m}{R_i}\right)^{2n}(\mu_r+1)-\left(\frac{R_m}{R_r}\right)^{2n}(\mu_r-1)\right]\\ +(nA^m_{z,n}+A^m_{z,n}+\mu_0M_{\vartheta n})\left[\left(\frac{R_r}{R_i}\right)^{2n}(\mu_r-1)-(\mu_r+1)\right]\\ +2\left(\frac{R_m}{R_r}\right)^{n-1}\left[(A^m_{z,n}+\mu_0M_{\vartheta n}+\mu_rnA^m_{z,n})+\left(\frac{R_r}{R_i}\right)^{n}(A^m_{z,n}+\mu_0M_{\vartheta n}-\mu_rnA^m_{z,n})\right]\end{array}}{\begin{array}{l}(\mu_r^2-1)\left[\left(\frac{R_s}{R_m}\right)^{2n}-\left(\frac{R_m}{R_i}\right)^{2n}+\left(\frac{R_r}{R_i}\right)^{2n}-\left(\frac{R_s}{R_r}\right)^{2n}\right]\\ +(\mu_r+1)^2\left[\left(\frac{R_s}{R_i}\right)^{2n}-1\right]+(\mu_r-1)^2\left[\left(\frac{R_m}{R_r}\right)^{2n}-\left(\frac{R_r}{R_i}\right)^{2n}\left(\frac{R_s}{R_m}\right)^{2n}\right]\end{array}}
\end{aligned}
\tag{19}
$$

$$
\begin{aligned}
f_{r,\mathrm{PM}}(r,n) &= \left(\frac{r}{R_s}\right)^{n-1}\left(\frac{R_m}{R_s}\right)^{n+1}+\left(\frac{R_m}{r}\right)^{n+1}\\
f_{r,out,\mathrm{PM}}(r,n) &= \left(\frac{r}{R_m}\right)^{n-1}+\left(\frac{R_s}{R_m}\right)^{n-1}\left(\frac{R_s}{r}\right)^{n+1}
\end{aligned}
\tag{20}
$$

The steps reported in Table 3 are equivalent to pre-conditioning the original system, yeilding

$$\boldsymbol{A}\boldsymbol{x} = \boldsymbol{b} \;\rightarrow\; \boldsymbol{A}\boldsymbol{P}^{-1}\boldsymbol{P}\boldsymbol{x} = \boldsymbol{b}, \tag{21}$$

where the different matrix/vectors are expressed as it follows, with the different pre-conditioner being used for the inrunner and the outrunner case (22)–(26), as shown at the bottom of the page.

In this way, $\boldsymbol{x}$ is the solution leading to the RFF while $\boldsymbol{P}\boldsymbol{x}$ leads to the OFF. This said, it is worth pointing out that other pre-conditioning solutions can be found in the literature. They are mostly based on normalizing the radius (r) in the RFF with a higher radius of the enclosing boundaries of the considered region (e.g., R_s in the airgap region of the inrunner topology) as mentioned in [13] and suggested in [26]. According to this rule, the pre-conditioners can be written as:

$$\boldsymbol{P}^{-1}_{IN,\,[26]} = diag\left(R_s^{-n+1},\, R_s^{n+1},\, R_m^{-n+1},\, R_m^{n+1},\, R_r^{-n+1},\, R_r^{n+1}\right) \tag{27}$$

$$\boldsymbol{P}^{-1}_{OUT,\,[26]} = diag\left(R_m^{-n+1},\, R_m^{n+1},\, R_r^{-n+1},\, R_r^{n+1},\, R_i^{-n+1},\, R_i^{n+1}\right) \tag{28}$$

The two resulting pre-conditioned systems are benchmarked against each other to assess the effectiveness of the pre-conditioners. This was done by computing the condition number of both the resulting conditioned matrices with respect to the outrunner case, as a function of the harmonic order (n). However, it was needed to set $R_i = R_r$ to avoid the existence of singularities in the pre-conditioned system obtained through [26]. Such a correction is not needed for the system from the OFF, which can handle the cases $R_i = Inf$ and $R_i = 0$. The condition number is computed as the product between the 2-norm of the matrix and its inverse. The result is reported in Fig. 3. The logarithm of the condition number is shown as it represents an indication of the loss of accuracy

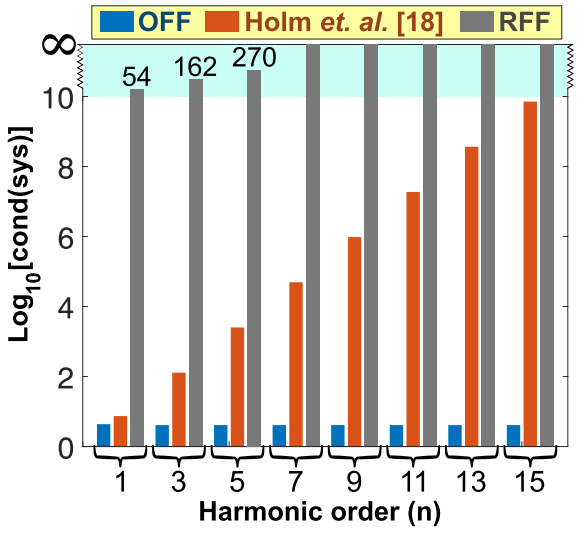

FIGURE 3. Logarithm of the condition number for the two pre-conditioned systems (21) referring to the no-load field solution for the outrunner case in Table 4: OFF in blue (preconditioner in (26)), normalized expressions according to [26] in red (preconditioner in (28)) and RFF in grey.

in decimal places by solving the system. However, the value resulting from an ill-conditioned matrix should be mistrusted as the inverse computation is inherently inaccurate.

Even though the solution proposed in [26] exhibits a better numerical behaviour than the RFF, which has a condition number diverging to infinite at low harmonic orders, it clearly represents a sub-optimal solution if compared to the OFF.

V. NUMERICAL SENSITIVITY ANALYSIS

The numerical analysis is performed in this section with respect to the magnets field solution. The RFF and the OFF are compared to address the different accuracy and the sensitivity to machine size. Two different cases are then taken and compared in terms of numerical accuracy of the different

$$\boldsymbol{x} = \left[A^{+}_{z,\mathrm{III}},\, A^{-}_{z,\mathrm{III}},\, A^{+}_{z,\mathrm{IV}},\, A^{-}_{z,\mathrm{IV}},\, A^{+}_{z,\mathrm{V}},\, A^{-}_{z,\mathrm{V}}\right]^{t} \tag{22}$$

$$\boldsymbol{b} = \left[0,\, A_{PM,r}(R_m),\, \frac{A_{PM,\vartheta}(R_m) + \mu_0\, M_{\vartheta n}}{n},\, A_{PM,r}(R_r),\, \frac{A_{PM,\vartheta}(R_r) + \mu_0\, M_{\vartheta n}}{n},\, 0\right]^{t} \tag{23}$$

$$\boldsymbol{A} = \begin{bmatrix} R_s^{n-1} & -R_s^{-n-1} & 0 & 0 & 0 & 0 \\ R_m^{n-1} & R_m^{-n-1} & -R_m^{n-1} & -R_m^{-n-1} & 0 & 0 \\ \mu_r R_m^{n-1} & -\mu_r R_m^{-n-1} & -R_m^{n-1} & R_m^{-n-1} & 0 & 0 \\ 0 & 0 & -R_r^{n-1} & -R_r^{-n-1} & R_r^{n-1} & R_r^{-n-1} \\ 0 & 0 & -R_r^{n-1} & R_r^{-n-1} & \mu_r R_r^{n-1} & -\mu_r R_r^{-n-1} \\ 0 & 0 & 0 & 0 & R_i^{n-1} & -R_i^{-n-1} \end{bmatrix} \tag{24}$$

$$\boldsymbol{P}^{-1}_{IN} = diag\left(R_s^{-n+1},\, R_m^{n+1},\, R_m^{-n+1},\, R_r^{n+1},\, R_r^{-n+1},\, R_i^{n+1}\right) \tag{25}$$

$$\boldsymbol{P}^{-1}_{OUT} = diag\left(R_m^{-n+1},\, R_s^{n+1},\, R_r^{-n+1},\, R_m^{n+1},\, R_i^{-n+1},\, R_r^{n+1}\right) \tag{26}$$

formulations. Since the numerical inaccuracy are affecting both radial and tangential components, the results will mostly refer to the radial component, without loss of generality.

A. MACHINE-SIZE SENSITIVITY

The sensitivity analysis is studied with respect to the machine size. It is mainly driven by the intuitive fact that one would expect the expressions shown in eq. (19) to be less prone to underflow/overflow when the radii values are around one meter. This analysis is performed on the two cases, whose parameters are listed in Table 4. The analysis is carried out by scaling the radii with the same coefficient, which is set to scale the two geometries from their original size up to a scaling factor giving an air gap radius of about 3.5 m for both the cases. The flux density in the middle of the airgap is processed for all the resulting geometries, and the percentage difference in the total harmonic distortion (THD) of the radial flux density component is computed for the OFF against the RFF. It is clear from eq. (20) that the use of the same scaling factor for all the radii maintains all the harmonics at the same value. Thus the OFF of the original geometries (i.e., unitary scaling factor) is considered as a reference for the error function defined as it follows.

$$err_{THD}\% = \frac{THD\left[B^{\mathrm{PM}}_{r,\mathrm{III,opt}}\right] - THD\left[B^{\mathrm{PM}}_{r,\mathrm{III,raw}}\right]}{THD\left[B^{\mathrm{PM}}_{r,\mathrm{III,opt}}\right]}100 \quad (29)$$

The results are shown in Fig. 3. The step variations of the error functions in the first part are due to the sudden numerical contribution of high-harmonic terms that were not represented. They were exhibiting underflow at smaller radii; vice versa, above one meter, the sudden variation is due to the gradual overflow of some high-harmonic terms in the RFF, causing an increase in the error. As expected, the error around one meter in size is negligible. It is worth noting that the RFF expressed in eq. (19) cannot be directly implemented for the out-runner case, since, according to Table 1, R_i must be set to infinity. For the sake of completeness, the coefficients of the RFF for the out-runner case are reported in Appendix C. Being the two RFFs numerically different from each other, the number of step variations in the error, with the size increase, is different (Fig. 4). Besides, the higher number of poles of the out-runner topology makes the error occurrence more remarkable, as the higher exponents amplify the underflow/overflow occurrence.

B. CASE-STUDY COMPARISON

The results from the two field formulations are now bench-marked against each other by considering the two case-studies presented in Table 4. With regard to the in-runner case in Table 4, the flux density waveform and its harmonic content are shown in Fig. 5 as a comparison between the two formulations. The FEA validation is also shown for the flux density waveform, ensuring the correctness of the solution. The mesh of the FE model was not optimized in detail as an objective in itself, but it was built to obtain a fine discretization in the airgap region to ensure the required accuracy for validation purposes. For both the inrunner and the outrunner case, the mid-airgap arc was discretized with 450 elements. In the final discretization, the airgap region over the simulated one-pole section counts 40752 elements with approximately 20 radial layers over the 1.4 mm airgap of the inrunner and 35926 elements with approximately 32 layers over the 1.5 mm airgap of the outrunner case. In addition, cubic elements were employed for both models.

Intuitively, the difference between the two formulations will show lower difference where higher-order harmonics are less significant, i.e., farther from the source of the field. In order to prove this, the field map obtained with the two formulations is shown in Fig. 6, along with the percentage

TABLE 4. SPM machines data (courtesy of Alva industries).

Parameter	*Machine specification*	
	In-runner air-cored single airgap	Out-runner air-cored double airgap
R_r	27.6 mm	99 mm
R_m	35.6 mm	93.5 mm
R_g	36.3 mm	92.8 mm
R_w	37 mm	92 mm
R_{wi}	40 mm	91 mm
R_s	40 mm	90 mm
R_i	0 mm	∞mm
l_a	70 mm	35 mm
B_r	1.35 T	1.4 T
μ_r	1	1
α_p	0.5	0.5
p	3	26
N_t	6	1
q	1	1
b	1	1
I	28 A	53 A

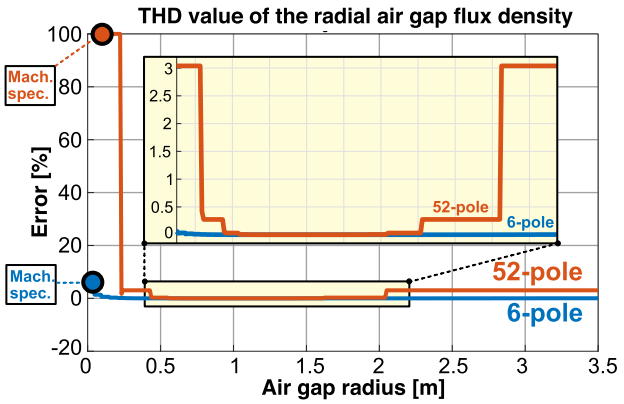

FIGURE 4. Percentage THD error of airgap radial no-load flux density of RFF, in the middle of the airgap ($r = R_g$), with the increase of the machine size. Original machine specifications in Table 4. The radii are scaled with the same factor.

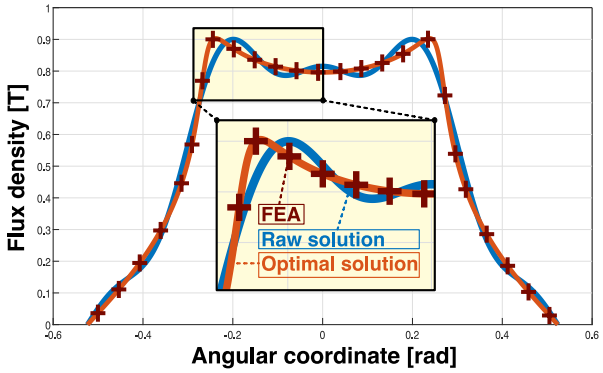

(a) Radial flux density waveform comparison in the middle of the airgap (r = R_g) over one pole pair (in-runner case in Table 4)

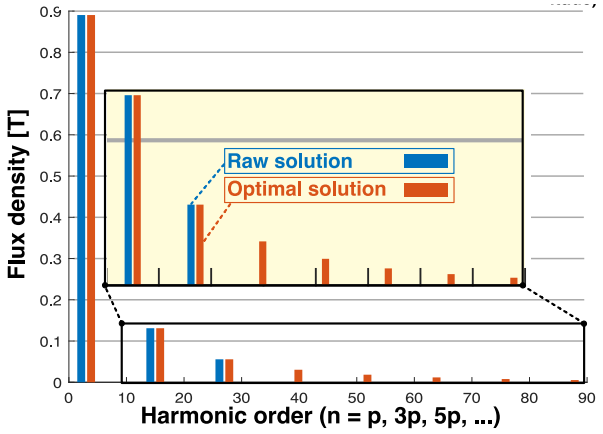

(b) Radial flux density harmonic content comparison in the middle of the airgap (r = R_g in-runner case in Table 4)

Fig. 5: Radial no-load flux density comparison in the middle

FIGURE 5. Radial no-load flux density comparison in the middle of the airgap ($r = R_g$ in-runner case in Table 4).

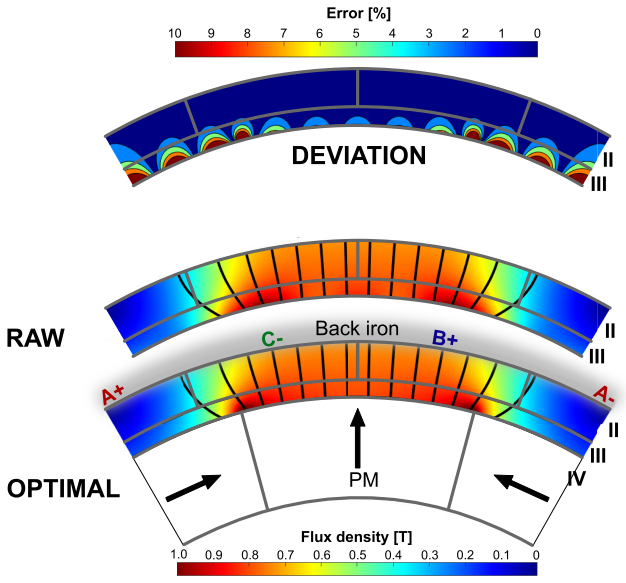

FIGURE 6. Comparison of the no-load flux density norm over the air gap and winding region for the RFF and the OFF, of the only PMs field (one pole section of the 6-pole in-runner case in Table 4)). Percentage error contour map on top; on the vicinity of the magnets boundary the maximum error is as high as 54%.

error between the two, which clearly highlights the latter statement.

The same analyses of airgap flux density waveform and maps are carried out for the out-runner case. Since the number of poles is much higher, the numerical inaccuracy of the RFF affects the solution already at low harmonic orders, thus, making it impossible to represent any harmonic but only the fundamental one. This is shown in Fig. 7, along with the FEA validation of the waveform. The field maps for the two formulations in the airgap/winding regions are shown in Fig. 8, and the error map shows the inaccuracy propagation of the RFF in the same region.

VI. MAGNETIC FIELD CONTRIBUTION FROM ARMATURE CURRENT

The two formulations for the stator winding field solution are here derived according to the hypotheses listed in Section III. The procedure for the field problem definition follows the one described in [28], [29], which is based on modeling the three-phase current density distribution as the source of the field.

$$J(\vartheta, t) = \sum_{h=p,7p,13p,\ldots}^{\infty} J_h \cos(h\vartheta - \omega t) + \sum_{k=5p,11p,17p,\ldots}^{\infty} J_k \cos(k\vartheta + \omega t) \quad (30)$$

Similarly to what has been done when considering the field contribution from the PMs (Section IV), to model the field solution from the stator winding, three different subdomains are considered again (as the magnets recoil permeability is assumed to be unitary). Now region III includes regions IV and V in Fig. 1. In region I and III the governing Laplace equation leads to the following solution:

$$A_z^{\mathrm{J}}(r, \vartheta, t) = \sum_{h=p,7p,13p,\ldots}^{\infty} (A_h^+ r^h + A_h^- r^{-h}) \cos(h\vartheta - \omega t) + \sum_{k=5p,11p,17p,\ldots}^{\infty} (A_k^+ r^k + A_k^- r^{-k}) \cos(k\vartheta + \omega t) \quad (31)$$

and from the governing Poisson's equation (5) in the winding region, a particular solution to the homogeneous one in (31) has to be added, yielding to the following expression [29]:

$$A_{z,\mathrm{II}}^J(r, \vartheta, t) = \sum_{h=p,7p,13p,\ldots}^{\infty} w_h(r) \cos(h\vartheta - \omega t) \ldots + \sum_{k=5,11,17,\ldots}^{\infty} w_k(r) \cos(k\vartheta + \omega t) \quad (32)$$

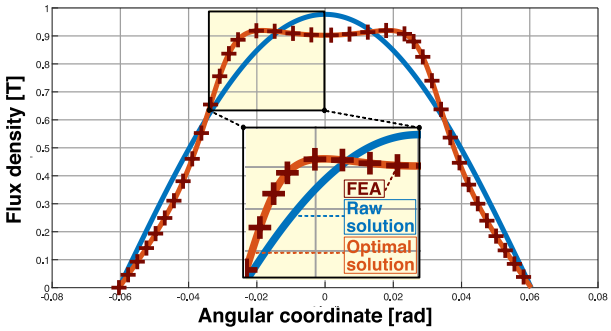

(a) Radial flux density waveform comparison in the middle of the airgap ($r = R_g$) over one pole pair (out-runner case in Table 4)

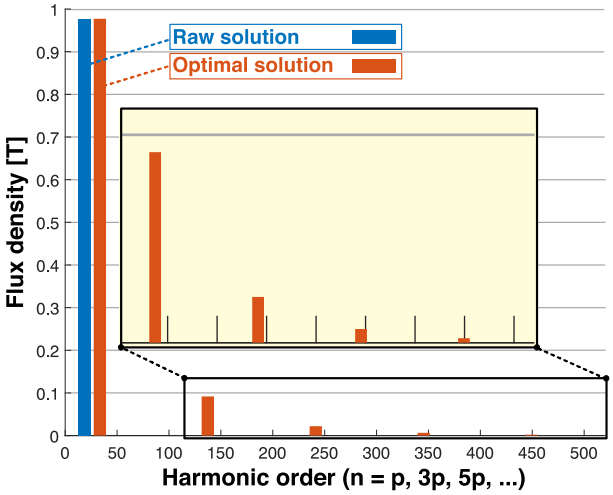

(b) Radial flux density harmonic content comparison in the middle of the airgap ($r = R_g$ out-runner case in Table 4)

FIGURE 7. Radial no-load flux density comparison in the middle of the airgap ($r = R_g$ out-runner case in Table 4).

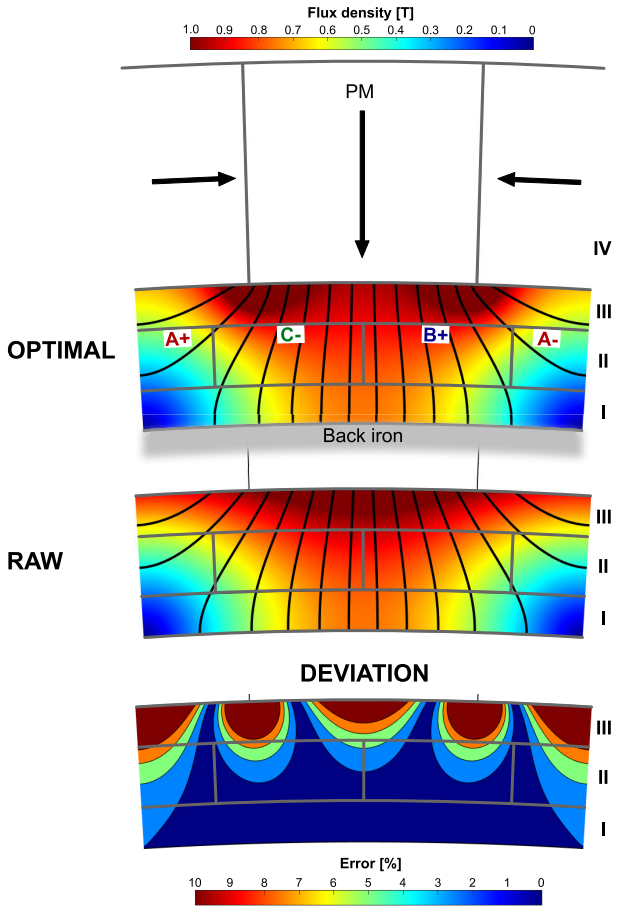

FIGURE 8. Comparison of the no-load flux density over the air gap and winding region with the RFF and the OFF for one pole pitch (52-pole out-runner case in Table 4)). Percentage error contour map to the right; on the vicinity of the magnets boundary the maximum error is as high as 68%.

where the terms $w_m(r)$ are reported in the Appendix D.

Through similar reasonings applied for the magnets field contribution, the following boundary conditions are now to be set for the armature field solution, between the three pre-defined regions:

$$H^{\mathrm{J}}_{\vartheta,\mathrm{I}}\Big|_{r=R_s} = 0 \tag{33}$$

$$\left(B^{\mathrm{J}}_{r,\mathrm{I}} = B^{\mathrm{J}}_{r,\mathrm{II}}\right)\Big|_{r=R_{wi}}, \quad \left(H^{\mathrm{J}}_{\vartheta,\mathrm{I}} = H^{\mathrm{J}}_{\vartheta,\mathrm{II}}\right)\Big|_{r=R_{wi}} \tag{34}$$

$$\left(B^{\mathrm{J}}_{r,\mathrm{II}} = B^{\mathrm{J}}_{r,\mathrm{III}}\right)\Big|_{r=R_w}, \quad \left(H^{\mathrm{J}}_{\vartheta,\mathrm{II}} = H^{\mathrm{J}}_{\vartheta,\mathrm{III}}\right)\Big|_{r=R_w} \tag{35}$$

$$H^{\mathrm{J}}_{\vartheta,\mathrm{III}}\Big|_{r=R_i} = 0 \tag{36}$$

The boundary conditions must hold at any angular coordinate ϑ, any time instant t and for any harmonic $m = \{h, k\}$. The resulting system of equations is here reported directly in matrix notation, both in its original form and the pre-conditioned one. The explicit expressions to build the system, can be deduced from eq. (58) and by using eqs. (31) and (32) arriving at the following (37)–(42), as shown at the bottom of the next page.

Yet again, the original system and the pre-conditioned one were solved in the Wolfram Cloud to obtain both the RFF and the OFF, respectively.

The lack of accuracy in the RFF follows the same exact criterion explained for the PM's field contribution. The pre-conditioned system is ready to be solved directly for an arbitrary number of harmonics, without falling into inaccurate solutions. In the same way, the closed-form solution itself can be extended to an arbitrary number of harmonics. The OFF's explicit expressions are here omitted for the sake of compactness but can be directly obtained from (37).

A. NUMERICAL PERFORMANCE COMPARISON

In so far as the airgap field solution is considered, the numerical inaccuracy of the OFF is less remarkable when compared to the PM field comparison. For this reason, the only field map from the OFF, and the deviation between the two formulations are shown as a result of the out-runner case in Fig. 9 (the time instant was set to $t = 0$).

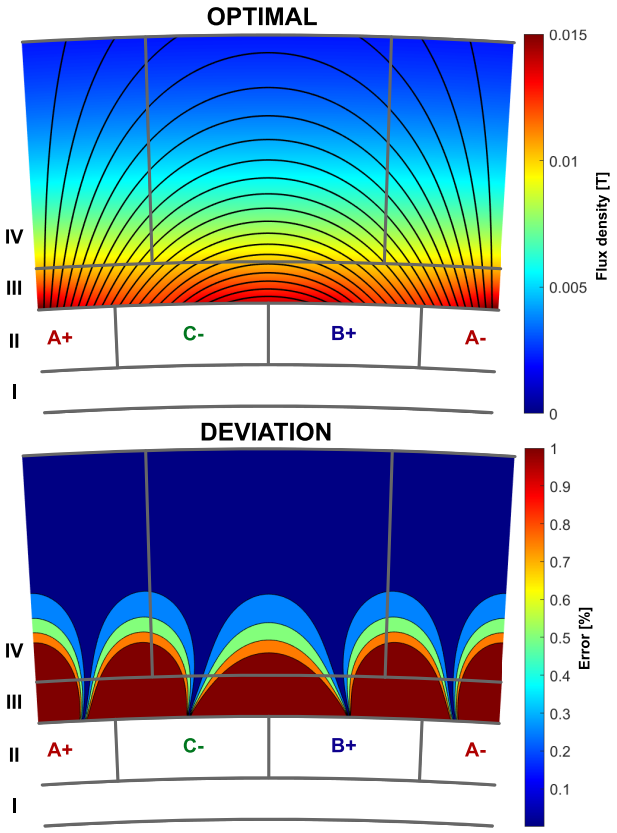

FIGURE 9. Error map for the armature field solution, for the outrunner case in Table 4, on the vicinity of the winding boundary (the maximum error is around 16%).

The error produced by the RFF, shows a negligible impact in the airgap region, despite the case with high number of poles should represent the worst case when it comes to the discrepancy between the results. However, it is worth pointing out that by moving into the winding region, the physical increase in the harmonic content, and more complicated closed-form expressions for the RFFs, make the deviation to become non-negligible. For instance, already in the vicinity of the winding boundary, the maximum relative error is as high as 16% (Fig. 9).

VII. IMPLICATION OF THE FINDINGS

In the previous sections, the deviation between the RFF and the OFF has been assessed. The impact of such a discrepancy may be more or less significant, depending on which application the analytical model is assigned to. In [39], [42], the analytical modeling of PM machines was employed for optimizing Halbach arrays by considering the harmonic content of the flux density as well. Moreover, in [32], the field solution in the region of the magnet was used for demagnetization analysis in Halbach arrays. For similar analyses, if carried out over a wide range of machine sizes, the use of OFF is paramount to prevent having flaw-full design procedures.

Other analyses that may be affected by inaccurate RFFs are those where the armature field solution is post-processed to perform some loss estimations. In [45], the winding field was adopted for estimating induced eddy-currents loss in the magnets for a slotted topology. To this aim, some real current waveforms were considered, meaning that the current density distribution of eq. (30) becomes a nested sum accounting for both space and time harmonics. For inverter-fed slotless machines, the typically high harmonic content of the current waveform [46] may require an accurate field solution in a wide space harmonic spectrum to achieve acceptable loss estimates.

It is therefore clear that the use of a OFF for analytical modeling is fundamental. The comparison between OFF and RFF was here presented only within the airgap region. This was needed to give a consistent explanation to the choice of the optimal pre-conditioner by looking at the closed-form field expressions as well. Nevertheless, the mathematical problem as framed in (21) for the PMs field and in (37) for the armature reaction field, allows to accurately solve the field problem in any region of the cases listed in Table 1.

$$\boldsymbol{W}\boldsymbol{y} = \boldsymbol{c} \;\rightarrow\; \boldsymbol{W}\boldsymbol{C}^{-1}\boldsymbol{C}\boldsymbol{y} = \boldsymbol{c} \tag{37}$$

$$\boldsymbol{y} = \left[A^{+}_{z,\mathrm{I}}\,,\, A^{-}_{z,\mathrm{I}}\,,\, A^{+}_{z,\mathrm{II}}\,,\, A^{-}_{z,\mathrm{II}}\,,\, A^{+}_{z,\mathrm{III}}\,,\, A^{-}_{z,\mathrm{III}}\right]^{t} \tag{38}$$

$$\boldsymbol{c} = \left[0\,,\, A^{J}_{m}R_{wi}\,,\, \frac{2A^{J}_{m}R_{wi}}{m}\,,\, A^{J}_{m}R_{w}\,,\, \frac{2A^{J}_{m}R_{w}}{m}\,,\, 0\right]^{t} \tag{39}$$

$$\boldsymbol{W} = \begin{bmatrix} R_s^{m-1} & -R_s^{-m-1} & 0 & 0 & 0 & 0 \\ R_{wi}^{m-1} & R_{wi}^{-m-1} & -R_{wi}^{m-1} & -R_{wi}^{-m-1} & 0 & 0 \\ R_{wi}^{m-1} & -R_{wi}^{-m-1} & -R_{wi}^{m-1} & R_{wi}^{-m-1} & 0 & 0 \\ 0 & 0 & -R_w^{m-1} & -R_w^{-m-1} & R_w^{m-1} & R_w^{-m-1} \\ 0 & 0 & -R_w^{m-1} & R_w^{-m-1} & R_w^{m-1} & -R_w^{-m-1} \\ 0 & 0 & 0 & 0 & R_i^{m-1} & -R_i^{-m-1} \end{bmatrix} \tag{40}$$

$$\boldsymbol{C}_{IN}^{-1} = diag\left(R_s^{-m+1}\,,\, R_{wi}^{m+1}\,,\, R_{wi}^{-m+1}\,,\, R_w^{m+1}\,,\, R_w^{-m+1}\,,\, R_i^{m+1}\right) \tag{41}$$

$$\boldsymbol{C}_{OUT}^{-1} = diag\left(R_{wi}^{-m+1}\,,\, R_s^{m+1}\,,\, R_w^{-m+1}\,,\, R_{wi}^{m+1}\,,\, R_i^{-m+1}\,,\, R_w^{m+1}\right) \tag{42}$$

TABLE 5. Useful functions for the field expressions in the magnets region.

	INRUNNER	OUTRUNNER
$f^+(r)=$	$(r/R_m)^{n-1}$	$(r/R_r)^{n-1}$
$f^-(r)=$	$(R_r/r)^{n+1}$	$(R_m/r)^{n+1}$
$f_z^+(r)=$	$R_m(r/R_m)^n$	$R_r(r/R_r)^n$
$f_z^-(r)=$	$R_r(R_r/r)^n$	$R_m(R_m/r)^n$

A. OFF IN REGIONS WITH ACTING SOURCES

As it was mentioned in the previous paragraph, it is desirable to obtain the OFF where a field source is acting. The PMs field contribution in the magnets region is considered in the following. The coefficients for the OFF in the magnets region can be obtained directly from the pre-conditioned system in eq. (21). Let $\boldsymbol{y} = \boldsymbol{Px}$ be the solution to the pre-conditioned system; the two flux density components and the one component magnetic vector potential can be expressed as it follows:

$$B_{r,\mathrm{IV}}^{\mathrm{PM}}(r,\vartheta) = \sum_n^{\infty} n[y(3)f^+(r) + y(4)f^-(r) + A_{\mathrm{PM,r}}(r)] \times \cos(n\vartheta) \tag{43}$$

$$B_{\vartheta,\mathrm{IV}}^{\mathrm{PM}}(r,\vartheta) = \sum_n^{\infty} [ny(3)f^+(r) - ny(4)f^-(r) + A_{\mathrm{PM},\vartheta}(r)] \times \sin(n\vartheta) \tag{44}$$

$$A_{z,\mathrm{IV}}^{\mathrm{PM}}(r,\vartheta) = \sum_n^{\infty} [y(3)f_z^+(r) + y(4)f_z^-(r) + A_{\mathrm{PM}}(r)] \times \sin(n\vartheta) \tag{45}$$

The coefficients $y(3)$ and $y(4)$ for the inrunner or outrunner case, have the same structure as $K_B(n)$ or $K_{B,out}(n)$ and are the natural outcome of the pre-conditioned system in eq. (21); therefore the explicit expressions are omitted for the sake of compactness. The homologous RFFs are reported in eqs. (63), (65), (12).

The need to truncate the Fourier series leads to the occurrence of the Gibbs phenomenon where the solution exhibits sudden variations in the magnetic quantities. This happens in the vicinity, and within the magnet's region, where the magnetization's sudden variation creates discontinuities that cause such a phenomenon. One can overcome this problem, as done in [27], where the $\sigma - approximation$ is adopted for representing the truncated series. This is done by multiplying the above written expressions (43)-(45) by the following factor (Lanczos σ factor):

$$\left[\frac{\sin(\pi n/n_{max})}{\pi n/n_{max}}\right]^3$$

The field map, including the field solution in the magnets region, is shown in Fig. 10, along with the deviation between the RFF and the OFF. It is interesting to notice how the error map is not continuous between magnets region and airgap region. And this finds an explanation in the different numerical structure of the RFF in the two regions.

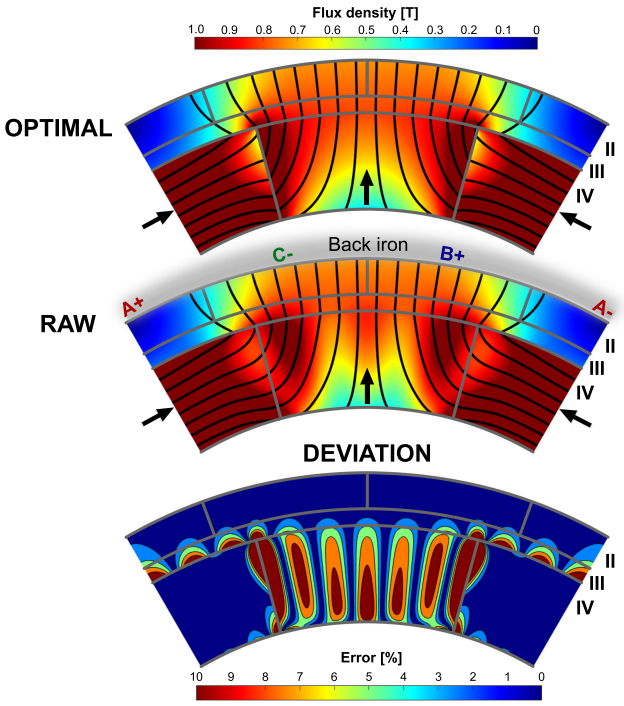

FIGURE 10. No-load field map comparison in airgap and magnets region (54% maximum error in the airgap region 57% maximum error in the magnets region). Inrunner machine parameters in Table 4.

B. ERROR PROPAGATION ON DERIVED QUANTITIES: ELECTROMAGNETIC TORQUE

The electromagnetic torque for a balanced three-phase machine can be computed as described in [41], [44] as the sum of the product of induced back-emf and current in each phase. This method is employed by convenience as the back-emf is another quantity to be computed. This technique is used here for both the topologies described in Table 4 regarding the OFF and the RFF. The computed torque through RFF is expected to deviate from the correct solution computed through OFF. This depends on as much as the error in the field map propagates within the winding region. This said, and considering Figs. 6 and 8, the deviation produced by the RFF in the torque computation is expected to be much more remarkable for the outrunner case. In order to prove this, the mentioned results are compared in Fig. 11.

The torque computed through RFF produces a little error already on the average value (0.75%). It cannot predict any ripple harmonics for the outrunner topology as opposed to the OFF. For the inrunner topology, the error on the average value and on the ripple is negligible although existent. In any case, the OFF produces consistently accurate results showing the main sixth harmonic on the torque typical of three-phase machines. As a further note, it was interesting to notice how integral quantities' evaluation shows a damping effect on the

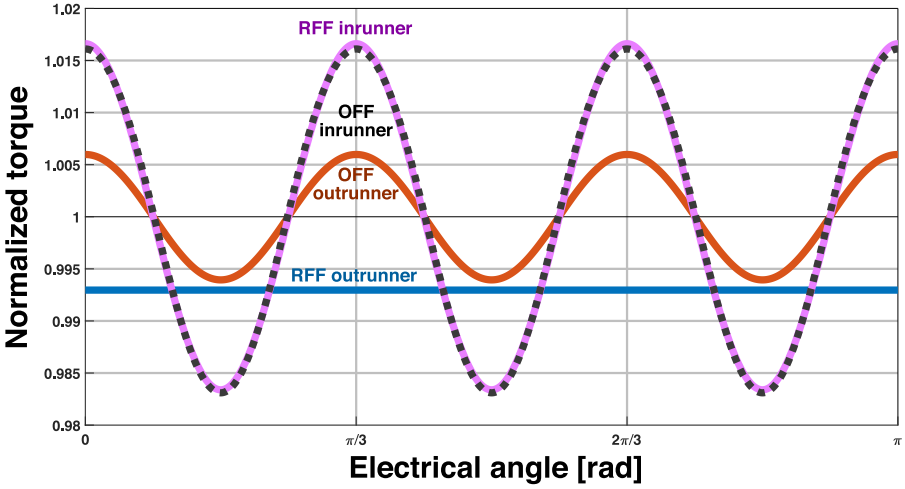

FIGURE 11. Normalized torque waveform over half electrical period revolution, computed through RFF and OFF for the two motor topologies in Table 4. The average OFF torque is used for normalization as follows: Outrunner with 11.00 Nm at 6.80 A/mm^2 rms loading and inrunner with 3.20 Nm at 2.95 A/mm^2 rms loading.

final error for as much as the integral is extended in parts of the domain where the deviation between the two formulations is less severe.

C. EXTENDING THE APPROACH TO SLOTTED TOPOLOGIES

A numerically optimized algebraic structure can always be achieved. In [34], [35], [38], subdomain modeling is adopted to model the saliency of surface inset PMs machines, and in [19], [47], [48], the same modeling criterion is employed for slotted topology. All these contributions share an optimized structure for the final formulation, which leads to the expected level of accuracy from the analytical field formulations. Only an insight will be given into the following issue of extending the proposed approach to slotted topologies, as of the complication of the problem formulation and the equations involved. In order to do this, [18] is taken as a reference as it considers a rather general model accounting for tooth tips as well. When treating a slotted topology, slot openings and slots constitute additional regions wherein the related governing equations are to be written. Slots and slot openings introduce additional harmonics in the problem; thus, sine and cosine harmonics coexist in the field formulations. Furthermore, slots and slot openings have their own harmonic orders when compared to the harmonics introduced by the source. These considerations make it more tedious to set up the boundary conditions between air-gap/slot-openings and slot-openings/slots as the field solution in one region has first to be expanded into Fourier series over the other region and vice versa. Nevertheless, one will end up obtaining a system of equations, which is ill-conditioned with respect to both the source harmonics and the slots/slot-openings ones. The optimal pre-conditioner implementation follows the same criterion, and the pre-conditioner will hold terms dependent on source space harmonics and slots/slot-openings harmonics. As in [18] the ill-conditioned nature of the problem was well known to the authors, the formulations where written in their well-conditioned form since the beginning. Therefore, no need for preconditioning the final system was needed. This, however, makes it hard to replicate or extend the solution since the OFF presented is not the natural outcome of the original problem. The closed-form expression for such a topology would inevitably be more complicated, and this justifies the fact that closed-form solutions are typically avoided for slotted topologies in the literature.

VIII. CONCLUSION

This paper investigates the geometrical sensitivity and accuracy level of the raw field formulation (RFF) for the analytical modeling of slotless PM machines. In this regard, the geometrical regions where the RFF corresponds to the optimized field formulation (OFF) has been identified. It is observed that the error increases for different machine sizes but depends on the number of poles as well. The general rule of thumb is never to use the directly obtained RFF to ensure the reproducibility of the analytical results. At the same time, a general rule for modeling of electrical machines is essential. Therefore, this paper developed a generalized algebraic approach to manipulate the field solution effectively for slotless topologies. A pre-conditioner is shown to obtain the OFF starting from the directly obtained RFF.

Consequently, the use of the right pre-conditioner allows extending the OFF in any region. The reason for adopting the optimal pre-conditioner was emphasized by comparing it with other suggested solutions in the literature. The issue was investigated by analyzing the system's condition number and highlighting the inaccuracy occurrence in the closed-form expressions. Moreover, an explicit solution to the Gibbs phenomenon is referred to as well. Thus, the accuracy level is

maximized in every region using the approach advocated in this paper.

For a future research item, the proposed methodology ought to be extended to slotted typologies. This will enhance the applicability of a unified optimal formulation. This, in turn, will give a sound rationale to the adoption of the optimal formulation in the literature, where the pre-conditioner being used is not explicitly reported.

ACKNOWLEDGMENT

The authors would like to thank Alva Industries, their industrial focus and recent developments on slotless machines have endorsed the implementation of the proposed models at their current level of detail. Thus, making it possible to highlight the presented issue.

APPENDIX A
MAGNETIZATION COMPONENTS OF THE TWO-SEGMENTS HALBACH ARRAY

Once α_p is defined as the mid-magnet to pole angle ratio:

$$\alpha_p = \frac{\alpha_m}{\pi/p}$$

coefficients M_{rn} and $M_{\vartheta n}$ for the mid-magnet can be determined through Fourier analysis of Fig. 2:

$$M_{rn}^{mid} = \frac{p}{\pi}\int_0^{2\pi/p} M_r(\vartheta)\cos(n\vartheta)\mathrm{d}\vartheta \tag{46}$$

$$M_{\vartheta n}^{mid} = \frac{p}{\pi}\int_0^{2\pi/p} M_\vartheta(\vartheta)\sin(n\vartheta)\mathrm{d}\vartheta \tag{47}$$

which can be simplified, thanks to the periodicity, and solved as it follows:

$$\begin{aligned} M_{rn}^{mid} &= \frac{4pB_{rem}}{\pi\mu_0}\int_0^{\alpha_p\frac{\pi}{2p}} \frac{1}{2}[\cos(\vartheta(1-n))+\cos(\vartheta(1+n))]\mathrm{d}\vartheta \\ &= \frac{B_{rem}}{\mu_0}\alpha_p(M_{1,n}+M_{2,n}) \end{aligned} \tag{48}$$

$$\begin{aligned} M_{\vartheta n}^{mid} &= \frac{4pB_{rem}}{\pi\mu_0}\int_0^{\alpha_p\frac{\pi}{2p}} -\frac{1}{2}[\cos(\vartheta(1-n))-\cos(\vartheta(1+n))]\mathrm{d}\vartheta \\ &= -\frac{B_{rem}}{\mu_0}\alpha_p(M_{1,n}-M_{2,n}) \end{aligned} \tag{49}$$

and the two coefficients $M_{1,n}$ and $M_{2,n}$ are defined as it follows:

$$M_{1,n} = \begin{cases} \dfrac{\sin\left[(n-1)\alpha_p\frac{\pi}{2p}\right]}{(n-1)\alpha_p\frac{\pi}{2p}} & \text{if } n \neq 1 \\ 1 & \text{if } n = 1 \end{cases} \tag{50}$$

$$M_{2,n} = \frac{\sin\left[(n+1)\alpha_p\frac{\pi}{2p}\right]}{(n+1)\alpha_p\frac{\pi}{2p}} \tag{51}$$

The same procedure applies to the side-magnets components as it follows:

$$\begin{aligned} M_{rn}^{side} &= \frac{4pB_{rem}}{\pi\mu_0}\int_{\frac{\alpha_p\pi}{2p}}^{\frac{\pi}{2p}} -\frac{1}{2}\left[\sin\left(\vartheta(1-n)-\frac{\pi}{2p}\right)+\ldots\right. \\ &\quad \left.\ldots+\sin\left(\vartheta(1+n)-\frac{\pi}{2p}\right)\right]\mathrm{d}\vartheta \\ &= \frac{B_{rem}}{\mu_0}\alpha_p(M_{3,n}-M_{4,n}) \end{aligned} \tag{52}$$

$$\begin{aligned} M_{\vartheta n}^{side} &= \frac{4pB_{rem}}{\pi\mu_0}\int_{\alpha_p\frac{\pi}{2p}}^{\frac{\pi}{2p}} -\frac{1}{2}\left[\sin\left(\vartheta(n-1)+\frac{\pi}{2p}\right)+\ldots\right. \\ &\quad \left.\ldots+\sin\left(\vartheta(1+n)-\frac{\pi}{2p}\right)\right]\mathrm{d}\vartheta \\ &= -\frac{B_r}{\mu_0}\alpha_p(M_{3,n}+M_{4,n}) \end{aligned} \tag{53}$$

and the two coefficients $M_{3,n}$ and $M_{4,n}$ are defined as it follows:

$$M_{3,n} = \begin{cases} \dfrac{\cos\left(\alpha_p\frac{\pi}{2p}(n-1)+\frac{\pi}{2p}\right)}{(n-1)\alpha_p\frac{\pi}{2p}} & \text{if } n \neq 1 \\ \left[\frac{1}{\alpha_p}-1\right] & \text{if } n = 1 \end{cases} \tag{54}$$

$$M_{4,n} = \frac{\cos\left(\alpha_p\frac{\pi}{2p}(n+1)-\frac{\pi}{2p}\right)}{(n+1)\alpha_p\frac{\pi}{2p}} \tag{55}$$

The resulting radial and circumferential magnetization components are therefore defined as:

$$M_{rn} = M_{rn}^{mid} + M_{rn}^{side} \tag{56}$$

$$M_{\vartheta n} = \pm(M_{\vartheta n}^{mid} + M_{\vartheta n}^{side}) \tag{57}$$

where the "+" is for inrunner (field focused externally) and the "-" for the outrunner (field focused internally).

APPENDIX B
FIELD EXPRESSIONS FROM PM CONTRIBUTION

From the definition of the flux density from the vector potential ($\boldsymbol{B} = \nabla \times \boldsymbol{A}$), the two components B_r and B_ϑ can be expressed as

$$B_r(r,\vartheta) = \frac{1}{r}\frac{\partial A_z}{\partial\vartheta}, \quad B_\vartheta(r,\vartheta) = -\frac{\partial A_z}{\partial r} \tag{58}$$

and from (4) the following expressions for magnetic field and flux density components can be deducted for each region of interest:

$$\begin{aligned} B_{r,\mathrm{III}}^{\mathrm{PM}} &= \frac{1}{r}\frac{\partial A_z^{\mathrm{PM}}}{\partial\vartheta} \\ &= \sum_n^\infty n[A_{z,\mathrm{III}}^{+}r^{n-1} + A_{z,\mathrm{III}}^{-}r^{-n-1}]\cos(n\vartheta) \end{aligned} \tag{59}$$

$$H_{r,\mathrm{III}}^{\mathrm{PM}} = \frac{1}{\mu_0}\frac{1}{r}\frac{\partial A_z^{\mathrm{PM}}}{\partial\vartheta}$$

$$= \sum_{n}^{\infty} \frac{n}{\mu_0}[A^{+}_{z,\mathrm{III}} r^{n-1} + A^{-}_{z,\mathrm{III}} r^{-n-1}] \cos(n\vartheta) \quad (60)$$

$$B^{\mathrm{PM}}_{\vartheta,\mathrm{III}} = -\frac{\partial A^{\mathrm{PM}}_{z}}{\partial r} = -\sum_{n}^{\infty} n[A^{+}_{z,\mathrm{III}} r^{n-1} - A^{-}_{z,\mathrm{III}} r^{-n-1}] \sin(n\vartheta) \quad (61)$$

$$H^{\mathrm{PM}}_{\vartheta,\mathrm{III}} = -\frac{1}{\mu_0}\frac{\partial A^{\mathrm{PM}}_{z}}{\partial r} = -\sum_{n}^{\infty} \frac{n}{\mu_0}[A^{+}_{z,\mathrm{III}} r^{n-1} - A^{-}_{z,\mathrm{III}} r^{-n-1}] \sin(n\vartheta) \quad (62)$$

$$B^{\mathrm{PM}}_{r,\mathrm{IV}} = \frac{1}{r}\frac{\partial A^{\mathrm{PM}}_{z,\mathrm{IV}}}{\partial \vartheta} = \sum_{n}^{\infty} n[A^{+}_{z,\mathrm{IV}} r^{n-1} + A^{-}_{z,\mathrm{IV}} r^{-n-1} + A_{\mathrm{PM},r}(r)] \times \cos(n\vartheta) \quad (63)$$

$$H^{\mathrm{PM}}_{r,\mathrm{IV}} = \frac{1}{\mu_0\mu_r}\left(\frac{1}{r}\frac{\partial A^{\mathrm{PM}}_{z,\mathrm{IV}}}{\partial \vartheta} - M_r\mu_0\right) = \sum_{n}^{\infty} \frac{n}{\mu_0\mu_r}[A^{+}_{z,\mathrm{IV}} r^{n-1} + A^{-}_{z,\mathrm{IV}} r^{-n-1} + \ldots + A_{\mathrm{PM},r}(r) - \mu_0 M_{rn}] \cos(n\vartheta) \quad (64)$$

$$B^{\mathrm{PM}}_{\vartheta,\mathrm{IV}} = -\frac{\partial A^{\mathrm{PM}}_{z,\mathrm{IV}}}{\partial r} = -\sum_{n}^{\infty}[nA^{m+}_{z,\mathrm{IV}} r^{n-1} - nA^{m-}_{z,\mathrm{IV}} r^{-n-1} + A_{\mathrm{PM},\vartheta}(r)] \times \sin(n\vartheta) \quad (65)$$

$$H^{\mathrm{PM}}_{\vartheta,\mathrm{IV}} = -\frac{1}{\mu_0\mu_r}\left(\frac{\partial A^{\mathrm{PM}}_{z,\mathrm{IV}}}{\partial r} + \mu_0 M_{\vartheta}\right) = -\sum_{n}^{\infty} \frac{1}{\mu_0\mu_r}[nA^{+}_{z,\mathrm{IV}} r^{n-1} - nA^{-}_{z,\mathrm{IV}} r^{-n-1} + \ldots + A_{\mathrm{PM},\vartheta}(r) + \mu_0 M_{\vartheta n}] \sin(n\vartheta) \quad (66)$$

where $A_{\mathrm{PM},r}(r)$ and $A_{\mathrm{PM},\vartheta}(r)$ are defined as:

$$A_{\mathrm{PM},r}(r) = \begin{cases} \dfrac{\mu_0(M_{\vartheta n} + nM_{rn})}{(n^2-1)} & \text{if } n \neq 1 \\ -\dfrac{\mu_0}{2}(M_{r1} + M_{\vartheta 1}) \cdot \ln(r) & \text{if } n = 1 \end{cases} \quad (67)$$

$$A_{\mathrm{PM},\vartheta}(r) = \begin{cases} \dfrac{\mu_0(M_{\vartheta n} + nM_{rn})}{(n^2-1)} & \text{if } n \neq 1 \\ -\dfrac{\mu_0}{2}(M_{r1} + M_{\vartheta 1})[\ln(r) + 1] & \text{if } n = 1 \end{cases} \quad (68)$$

$$B^{\mathrm{PM}}_{r,\mathrm{V}} = \frac{1}{r}\frac{\partial A^{\mathrm{PM}}_{z}}{\partial \vartheta} = \sum_{n}^{\infty} n[A^{+}_{z,\mathrm{V}} r^{n-1} + A^{-}_{z,\mathrm{V}} r^{-n-1}] \cos(n\vartheta) \quad (69)$$

$$H^{\mathrm{PM}}_{r,\mathrm{V}} = \frac{1}{\mu_0}\frac{1}{r}\frac{\partial A^{\mathrm{PM}}_{z}}{\partial \vartheta} = -\sum_{n}^{\infty} \frac{n}{\mu_0}[A^{+}_{z,\mathrm{V}} r^{n-1} + A^{-}_{z,\mathrm{V}} r^{-n-1}] \cos(n\vartheta) \quad (70)$$

$$B^{\mathrm{PM}}_{\vartheta,\mathrm{V}} = -\frac{\partial A^{\mathrm{PM}}_{z}}{\partial r} = -\sum_{n}^{\infty} n[A^{+}_{z,\mathrm{V}} r^{n-1} - A^{-}_{z,\mathrm{V}} r^{-n-1}] \sin(n\vartheta) \quad (71)$$

$$H^{\mathrm{PM}}_{\vartheta,\mathrm{V}} = -\frac{1}{\mu_0}\frac{\partial A^{\mathrm{PM}}_{z}}{\partial r} = -\sum_{n}^{\infty} \frac{n}{\mu_0}[A^{+}_{z,\mathrm{V}} r^{n-1} - A^{-}_{z,\mathrm{V}} r^{-n-1}] \sin(n\vartheta) \quad (72)$$

APPENDIX C
RAW FORMULATION COEFFICIENTS FOR THE OUT-RUNNER CASE

$$A^{+}_{z,\mathrm{III}} = \frac{\begin{array}{l} R^{n}_{m}\{-R^{2n+1}_{m}(\mu_r - 1)(nA^{m}_{z,n} - \mu_0 M_{\vartheta n} - A^{m}_{z,n}) \\ -R_m R^{2n}_{r}(\mu_r + 1)(nA^{m}_{z,n} + \mu_0 M_{\vartheta n} + A^{m}_{z,n}) \\ +2R^{n}_{m}R^{1+n}_{r}(A^{m}_{z,n} + \mu_r nA^{m}_{z,n} + \mu_0 M_{\vartheta n})\} \end{array}}{\begin{array}{l} n\{R^{4n}_{m}(\mu_r - 1)^2 - R^{2n}_{m}R^{2n}_{r}(\mu_r + 1)^2 \\ -R^{2n}_{s}R^{2n}_{m}(\mu_r + 1)(\mu_r - 1) \\ +R^{2n}_{r}R^{2n}_{s}(\mu_r - 1)(\mu_r + 1)\} \end{array}}$$

$$A^{+}_{z,\mathrm{III}} = R^{2n}_{s} A^{+}_{z,\mathrm{III}} \quad (73)$$

APPENDIX D
ARMATURE FIELD COEFFICIENTS

The expressions of $w_m(r)$ in (32) are obtained from the method of separation of variables, by treating separately the one case which would otherwise exhibit a singularity (i.e. $hp = 2$ namely fundamental component of a four-pole machine):

$$w_m(r) = \begin{cases} A^{+}_{m,\mathrm{II}} r^{m} + A^{-}_{m,\mathrm{II}} r^{-m} + A^{J}_{m} r^{2} & \text{if } m \neq 2 \\ A^{+}_{2,\mathrm{II}} r^{2} + A^{-}_{2,\mathrm{II}} r^{-2} + A^{J}_{2} r^{2} \ln(r) & \text{if } m = 2 \end{cases} \quad (74)$$

with $A^{J}_{m,\mathrm{II}}$ defined as:

$$A^{J}_{m} = \begin{cases} \dfrac{\mu_0 J_m}{m^2 - 4} & \text{if } m \neq 2 \\ -\dfrac{\mu_0 J_2}{4} & \text{if } m = 2 \end{cases} \quad (75)$$

and J_m representing the current density harmonics amplitudes in (30) as in [28]:

$$J_m = \frac{36}{\pi^2}\frac{p^2 N_t q I}{b|R^2_{wi} - R^2_{w}|} \sin\left(\frac{m\pi}{6p}\right)\frac{1}{m} \quad (76)$$

REFERENCES

[1] M. S. Islam, R. Mikail, and I. Husain, "Slotless lightweight motor for aerial applications," *IEEE Trans. Ind. Appl.*, vol. 55, no. 6, pp. 5789–5799, Nov. 2019.

[2] D. Lee, A. Yoon, S. Sirimanna, S. Salon, and K. S. Haran, "Impact of manufacturing tolerances on a low-reactance slotless PM synchronous machine," *IEEE Trans. Energy Convers.*, vol. 35, no. 1, pp. 366–374, Mar. 2020.
[3] A. Tuysuz, F. Meyer, M. Steichen, C. Zwyssig, and J. W. Kolar, "Advanced cooling methods for high-speed electrical machines," *IEEE Trans. Ind. Appl.*, vol. 53, no. 3, pp. 2077–2087, May 2017.
[4] Z. Song, C. Liu, K. Feng, H. Zhao, and J. Yu, "Field prediction and validation of a slotless segmented-Halbach permanent magnet synchronous machine for more electric aircraft," *IEEE Trans. Transport. Electrific.*, vol. 6, no. 4, pp. 1577–1591, Dec. 2020.
[5] M. Shao, G. Liu, Q. Chen, W. Zhao, and D. Zhang, "A lumped parameter magnetic circuit model for fault-tolerant machine with Halbach magnetized permanent-magnet," in *Proc. Int. Conf. Electr. Mach. Syst. (ICEMS)*, Oct. 2013, pp. 1174–1178.
[6] A. Chebak, P. Viarouge, and J. Cros, "Analytical model for design of high-speed slotless brushless machines with SMC stators," in *Proc. IEEE Int. Electric Mach. Drives Conf.*, vol. 1, May 2007, pp. 159–164.
[7] N. Boules, "Two-dimensional field analysis of cylindrical machines with permanent magnet excitation," *IEEE Trans. Ind. Appl.*, vol. IA-20, no. 5, pp. 1267–1277, Sep. 1984.
[8] E. Ilhan, B. L. J. Gysen, J. J. H. Paulides, and E. A. Lomonova, "Analytical hybrid model for flux switching permanent magnet machines," *IEEE Trans. Magn.*, vol. 46, no. 6, pp. 1762–1765, Jun. 2010.
[9] J. Wang and D. Howe, "Design optimization of radially magnetized, iron-cored, tubular permanent-magnet machines and drive systems," *IEEE Trans. Magn.*, vol. 40, no. 5, pp. 3262–3277, Sep. 2004.
[10] P. Jalali, S. T. Boroujeni, and N. Bianchi, "Analytical modeling of slotless eccentric surface-mounted PM machines using a conformal transformation," *IEEE Trans. Energy Convers.*, vol. 32, no. 2, pp. 658–666, Jun. 2017.
[11] S. T. Boroujeni, S. P. Emami, and P. Jalali, "Analytical modeling of eccentric PM-inset machines with a slotless armature," *IEEE Trans. Energy Convers.*, vol. 34, no. 3, pp. 1466–1474, Sep. 2019.
[12] J. T. Li, Z. J. Liu, and L. H. A. Nay, "Effect of radial magnetic forces in permanent magnet motors with rotor eccentricity," *IEEE Trans. Magn.*, vol. 43, no. 6, pp. 2525–2527, Jun. 2007.
[13] B. L. J. Gysen, K. J. Meessen, J. J. H. Paulides, and E. A. Lomonova, "General formulation of the electromagnetic field distribution in machines and devices using Fourier analysis," *IEEE Trans. Magn.*, vol. 46, no. 1, pp. 39–52, Jan. 2010.
[14] H. Tiegna, Y. Amara, and G. Barakat, "Overview of analytical models of permanent magnet electrical machines for analysis and design purposes," *Math. Comput. Simul.*, vol. 90, pp. 162–177, Apr. 2013.
[15] E. Devillers, J. Le Besnerais, T. Lubin, M. Hecquet, and J.-P. Lecointe, "A review of subdomain modeling techniques in electrical machines: Performances and applications," in *Proc. 22nd Int. Conf. Electr. Mach. (ICEM)*, Sep. 2016, pp. 86–92.
[16] J. Fu and C. Zhu, "Subdomain model for predicting magnetic field in slotted surface mounted permanent-magnet machines with rotor eccentricity," *IEEE Trans. Magn.*, vol. 48, no. 5, pp. 1906–1917, May 2012.
[17] L. J. Wu, Z. Q. Zhu, D. Staton, M. Popescu, and D. Hawkins, "Subdomain model for predicting armature reaction field of surface-mounted permanent-magnet machines accounting for tooth-tips," *IEEE Trans. Magn.*, vol. 47, no. 4, pp. 812–822, Apr. 2011.
[18] L. J. Wu, Z. Q. Zhu, D. Staton, M. Popescu, and D. Hawkins, "An improved subdomain model for predicting magnetic field of surface-mounted permanent magnet machines accounting for tooth-tips," *IEEE Trans. Magn.*, vol. 47, no. 6, pp. 1693–1704, Jun. 2011.
[19] Z. Q. Zhu, L. J. Wu, and Z. P. Xia, "An accurate subdomain model for magnetic field computation in slotted surface-mounted permanent-magnet machines," *IEEE Trans. Magn.*, vol. 46, no. 4, pp. 1100–1115, Apr. 2010.
[20] Z. Zhang, C. Xia, H. Wang, and T. Shi, "Analytical field calculation and analysis of surface inset permanent magnet machines with high saliency ratio," *IEEE Trans. Magn.*, vol. 52, no. 12, pp. 1–12, Dec. 2016.
[21] A. Ghaffari, A. Rahideh, H. Moayed-Jahromi, A. Vahaj, A. Mahmoudi, and W. L. Soong, "2-D analytical model for outer-rotor consequent-pole brushless PM machines," *IEEE Trans. Energy Convers.*, vol. 34, no. 4, pp. 2226–2234, Dec. 2019.
[22] T. Lubin, S. Mezani, and A. Rezzoug, "Exact analytical method for magnetic field computation in the air gap of cylindrical electrical machines considering slotting effects," *IEEE Trans. Magn.*, vol. 46, no. 4, pp. 1092–1099, Apr. 2010.
[23] P.-D. Pfister and Y. Perriard, "Slotless permanent-magnet machines: General analytical magnetic field calculation," *IEEE Trans. Magn.*, vol. 47, no. 6, pp. 1739–1752, Jun. 2011.
[24] B. Hannon, P. Sergeant, and L. Dupre, "Two-dimensional Fourier-based modeling of electric machines," in *Proc. IEEE Int. Electr. Mach. Drives Conf. (IEMDC)*, May 2017, pp. 1–8.
[25] Z. P. Xia, Z. Q. Zhu, and D. Howe, "Analytical magnetic field analysis of Halbach magnetized permanent-magnet machines," *IEEE Trans. Magn.*, vol. 40, no. 4, pp. 1864–1872, Jul. 2004.
[26] S. R. Holm, H. Polinder, and J. A. Ferreira, "Analytical modeling of a permanent-magnet synchronous machine in a flywheel," *IEEE Trans. Magn.*, vol. 43, no. 5, pp. 1955–1967, May 2007.
[27] C. Custers, J. Jansen, M. van Beurden, and E. Lomonova, "3D harmonic modeling of eddy currents in segmented conducting structures," *COMPEL-Int. J. Comp. Math. Electr. Electron. Eng.*, vol. 38, no. 1, pp. 2–23, 2019.
[28] A. Tessarolo, L. Branz, and C. Bruzzese, "A compact analytical expression for the load torque in surface permanent-magnet machines with slotless stator design," in *Proc. IEEE Workshop Electr. Mach. Design, Control Diagnosis (WEMDCD)*, Mar. 2013, pp. 8–17.
[29] A. Tessarolo, M. Bortolozzi, and C. Bruzzese, "Explicit torque and back EMF expressions for slotless surface permanent magnet machines with different magnetization patterns," *IEEE Trans. Magn.*, vol. 52, no. 8, pp. 1–15, Aug. 2016.
[30] S. T. Boroujeni and H. B. Naghneh, "Analytical modelling and prototyping a slotless surface-inset PM machine," *IET Electr. Power Appl.*, vol. 11, no. 3, pp. 312–322, Mar. 2017.
[31] J. Ofori-Tenkorrang and J. H. Lang, "A comparative analysis of torque production in Halbach and conventional surface-mounted permanent-magnet synchronous motors," in *Proc. Conf. Rec. IEEE Ind. Appl. Conf. 13th IAS Annu. Meeting (IAS)*, vol. 1, Oct. 1995, pp. 657–663.
[32] M. Galea, L. Papini, H. Zhang, C. Gerada, and T. Hamiti, "Demagnetization analysis for Halbach array configurations in electrical machines," *IEEE Trans. Magn.*, vol. 51, no. 9, pp. 1–9, Sep. 2015.
[33] N. Bianchi, S. Bolognani, and F. Luise, "Analysis and design of a brushless motor for high speed operation," in *Proc. IEEE Int. Electr. Mach. Drives Conf. (IEMDC)*, vol. 1, 2003, pp. 44–51.
[34] A. Rahideh and T. Korakianitis, "Analytical armature reaction field distribution of slotless brushless machines with inset permanent magnets," *IEEE Trans. Magn.*, vol. 48, no. 7, pp. 2178–2191, Jul. 2012.
[35] A. Rahideh and T. Korakianitis, "Analytical magnetic field distribution of slotless brushless machines with inset permanent magnets," *IEEE Trans. Magn.*, vol. 47, no. 6, pp. 1763–1774, Jun. 2011.
[36] Z. Q. Zhu, D. Howe, and C. C. Chan, "Improved analytical model for predicting the magnetic field distribution in brushless permanent-magnet machines," *IEEE Trans. Magn.*, vol. 38, no. 1, pp. 229–238, 2002.
[37] Z. Q. Zhu, D. Howe, E. Bolte, and B. Ackermann, "Instantaneous magnetic field distribution in brushless permanent magnet DC motors. I. Open-circuit field," *IEEE Trans. Magn.*, vol. 29, no. 1, pp. 124–135, Jan. 1993.
[38] A. Rahideh, M. Mardaneh, and T. Korakianitis, "Analytical 2-D calculations of torque, inductance, and back-EMF for brushless slotless machines with surface inset magnets," *IEEE Trans. Magn.*, vol. 49, no. 8, pp. 4873–4884, Aug. 2013.
[39] Y. Shen and Z. Zhu, "General analytical model for calculating electromagnetic performance of permanent magnet brushless machines having segmented Halbach array," *IET Electr. Syst. Transp.*, vol. 3, no. 3, pp. 57–66, Sep. 2013.
[40] Y. Shen and Z. Q. Zhu, "Investigation of permanent magnet brushless machines having unequal-magnet height pole," *IEEE Trans. Magn.*, vol. 48, no. 12, pp. 4815–4830, Dec. 2012.
[41] Y. Shen, G. Y. Liu, Z. P. Xia, and Z. Q. Zhu, "Determination of maximum electromagnetic torque in PM brushless machines having two-segment Halbach array," *IEEE Trans. Ind. Electron.*, vol. 61, no. 2, pp. 718–729, Feb. 2014.
[42] Y. Ni, Y. Liu, and Q. Wang, "Magnetic field analysis and optimisation of permanent magnet machineswith novel two-segment Halbach array," *IET Electr. Power Appl.*, vol. 13, no. 9, pp. 1355–1364, Sep. 2019.
[43] Z. Q. Zhu, "Recent development of Halbach permanent magnet machines and applications," in *Proc. Power Convers. Conf. Nagoya*, Apr. 2007, pp. K-9–K-16.
[44] S. G. Min, "Modeling, investigation, and minimization of AC winding loss in slotless PM machines," *IEEE Trans. Energy Convers.*, early access, Jan. 8, 2021, doi: 10.1109/TEC.2021.3050251.

[45] Z. Q. Zhu, K. Ng, N. Schofield, and D. Howe, "Improved analytical modelling of rotor eddy current loss in brushless machines equipped with surface-mounted permanent magnets," *IEE Proc. Electr. Power Appl.*, vol. 151, no. 6, pp. 641–650, Nov. 2004.
[46] M. Leandro, N. Bianchi, M. Molinas, and R. B. Ummaneni, "Low inductance effects on electric drives using slotless permanent magnet motors: A framework for performance analysis," in *Proc. IEEE Int. Electr. Mach. Drives Conf. (IEMDC)*, May 2019, pp. 1099–1105.
[47] A. Vahaj, A. Rahideh, H. Moayed-Jahromi, and A. Ghaffari, "Exact two-dimensional analytical calculations for magnetic field, electromagnetic torque, UMF, back-EMF, and inductance of outer rotor surface inset permanent magnet machines," *Math. Comput. Appl.*, vol. 24, no. 1, p. 24, Feb. 2019.
[48] L. J. Wu, Z. Q. Zhu, D. Staton, M. Popescu, and D. Hawkins, "Analytical model of eddy current loss in windings of permanent-magnet machines accounting for load," *IEEE Trans. Magn.*, vol. 48, no. 7, pp. 2138–2151, Jul. 2012.

MATTEO LEANDRO (Member, IEEE) received the M.Sc. degree in electrical energy engineering from the University of Padova, Padua, Italy, in 2019. He is currently pursuing the Ph.D. degree with the Department of Electric Power Engineering, Norwegian University of Science and Technology (NTNU), Trondheim, Norway. He is cooperating closely with Alva Industries AS, Trondheim, where his research is applied to analytical modeling and digital twin development of electric drives using slotless machines. The aim is to move toward development of lightweight coreless machines for aerial propulsion systems. His current research interests include analytical formulations for electrical machine analysis, slotless machines, and multiphysics. He regularly serves as a reviewer for several IEEE journals and conferences.

JONAS KRISTIANSEN NØLAND (Member, IEEE) was born in Drammen, Norway, in 1988. He received the M.Sc. degree in electric power engineering from the Chalmers University of Technology, Gothenburg, Sweden, in 2013, and the Ph.D. degree in engineering physics from Uppsala University, Uppsala, Sweden, in 2017.

In 2017, he was an Associate Professor with the University of South-Eastern Norway (USN). Since December 2018, he has been an Associate Professor with the Department of Electric Power Engineering, Norwegian University of Science and Technology (NTNU). His current research interests include excitation systems, improved utilization of electrical machines, high-power machinery for aircraft applications, and transportation electrification in general.

Dr. Nøland is a member of the IEEE Transportation Electrification Community (TEC), the IEEE Industrial Electronics Society (IES), the IES Electric Machines Technical Committee, the IEEE Industry Applications Society (IAS), and the IEEE Power and Energy Society (PES). He is also a Board Member of the Norwegian Academic Committee of Publication in Technology in Electrical Power Engineering and the Vice-Chair of the IEEE Power and Energy Chapter of Norway. He currently serves as an Editor for the IEEE TRANSACTIONS ON ENERGY CONVERSION and as an Associate Editor for the IEEE TRANSACTIONS ON INDUSTRIAL ELECTRONICS.